Pergamon

Adv. Space Res. Vol. 15, No. 8/9, pp. (8/9)181–(8/9)223, 1995

0273–1177/95 $9.50 + 0.00

0273-1177(94)00101-4

A REVIEW OF THE PHYSICS OF ELECTRON HEATING AT COLLISIONLESS SHOCKS

J. D. Scudder

Department of Physics and Astronomy, University of Iowa, Iowa City, IA 52242, U.S.A.

ABSTRACT

The current understanding of the increase of electron temperature across fast and slow magnetosonic collisionless shocks observed in space is reviewed. The concept advanced by Goodrich and Scudder /1/ that the electron temperature increase is essentially caused by the inflation of the phase space in the presence of the DC deHoffmann-Teller (HT) /2/ electric field within the shock layer has achieved wide acceptance. This review reiterates the essential basis of that work: that with their relatively small inertia the electrons remain magnetized while the ions do not. It is this fact that makes the HT frame the relevant one for electron energetics. Subsequent discussions of the electron issues and its corollaries always come back to the same issue: $m/M \ll 1$ makes collisionless shocks the way they are observed. The predicted corollaries of this understanding in terms of the diagnostic signatures in the magnetic field within the shock structure have been challenged in the intervening years, but nevertheless confirmed by independent groups. This understanding has also been transferred to the relatively rare slow shocks. These corollaries concern the geometry of magnetic tubes of force that underlie the one-fluid $\mathbf{J} \times \mathbf{B}$ force. This geometry clarifies that the tubes of force that pierce the shock do not lie in a single coplanarity plane, but meander in a staircase-like fashion between distinct asymptotic coplanarity planes perpendicular to the tangential electric field direction, $\mathbf{E_T}$. It is also developed that the relative size of the deHoffmann-Teller and Normal Incidence cross shock electrical potential is now established, with the Normal Incidence potential jump bigger (smaller) than the deHoffmann-Teller jump in observed fast (slow) shock waves. A geometrical discussion has been made in this review that these relations are consistent with the required tangential torques needed for the ion deflections required by Hugoniot, being opposite for the fast and slow shocks. Computer simulations with particle electrons have just recently been able to verify the experimental picture summarized above, including the self-consistent generation of the strong shock flat-topped electron distribution functions and the relatively unimportant role of instabilities in electron *heating* as opposed to *assimilation or scattering*. The diagnostics of this code have supported the overwhelming importance of the DC effects of the coherent forces in the electron shock heating physics.

INTRODUCTION

The changes of electron properties across collisionless shocks in space have been measured for more than twenty-five years /3,4/. Since that time it has been repeatedly confirmed that (1) the changes in the electron temperature at collisionless shocks in space are less dramatic than for the ions; and (2) that in the case of the strong fast shock at the earth's bow wave, the velocity distribution function, $f(\mathbf{v})$, immediately behind the ramp in the magnetic intensity was more or less isotropic with a flat-top (cf. Figure 1 from Vela and OGO-V measurements acquired in 1968). Similar features were reported at bow shocks of the planets, the magnetotail, and under extraordinary circumstances in the interplanetary medium. The reported information on electrons for interplanetary shocks is exclusively about the omnipresent fast magnetosonic shocks, since the extremely rare interplanetary slow shocks invariably have not been sampled by the less frequently

flown electron detectors. Recent information has been forthcoming about electron behavior near slow shocks in the magnetospheric system from the ISEE data set.

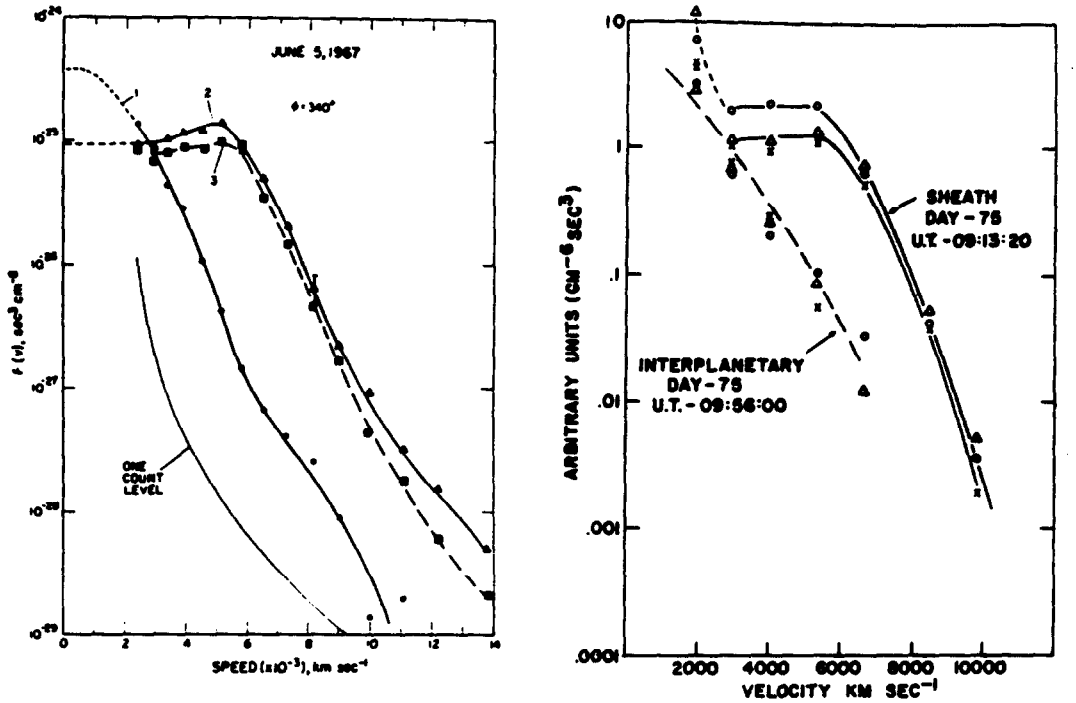

Fig. 1. Flat-topped distributions Vela /3/ and OGO-5 /4/. In both examples multiple cuts are exhibited to show the flat-top extent in velocity space: cuts 2 and 3 in the left-hand drawing; traces with x's, triangles, and o's in the right-hand example. For reference the cooler interplanetary distribution is shown labeled 1 in the left Vela example and as labeled in the OGO example. The sharp upturn at low energies indicated on the right panel is the ambient photoelectrons.

There were many suggestions for microinstabilities that were surmised as the cause of the observed heating of the electrons. A popular family of instabilities were those of the ion-acoustic type /5/ with free energy derived from the assumed large cross field ramp drift of electrons relative to the ions. The physical scale lengths at shock layers were poorly known; what was the precursor, what was the layer proper, or the downstream regimes of thermalization were clouded by space-time ambiguities. A phase standing, but inhomogeneous, structure was as equally tenable as a "turbulent" intrinsically time dependent structure. Theoreticians were left with a relatively unconstrained set of observational facts. Impressions garnered from time series left considerable room for theoretical explanations of the ion and the relatively trivial amount of electron shock heating.

Without spatial measurements of the thickness of layers, only integrated currents, ΔI could be deduced

$$\Delta I_y = \frac{c}{4\pi}\Delta B_z \equiv \frac{c}{4\pi}[B_z]\,. \tag{1a}$$

Current densities constrain relative drifts, yet they are unavailable from magnetic field profiles alone. Independent information of the spatial scale Δx of the change in B_z, denoted $[B_z]$, or separate detection of the electron and ion vectorial number fluxes within the shock layer are needed to constrain relative drift rates, viz.:

$$J_y = \frac{\Delta I_y}{\Delta x} = -n\,e\,(\mathbf{V_e} - \mathbf{V_i})\cdot\hat{\mathbf{y}}\,. \tag{1b}$$

In this early period neither Δx nor $\mathbf{V_e} - \mathbf{V_i}$ were known. Had thicknesses been known the transit time for particles would have been also then known, giving upper time limits for instabilities to be effective in producing the observed heating. In this period there was only the loosest of constraints. It should also be mentioned that in this exploratory phase, the *only* question seemed to be how to complete the early paradigm: "... what microinstabilities take the place of collisions to allow the shock to form?" /6/.

Without particle detectors that can determine *where* the plasma slows down in a model independent way, the *location* of *the* shock and low- and high-entropy sides could not be unambiguously identified nor its thickness determined. This problem was particularly difficult at the quasi-standing earth/planetary bow shocks where the ion plasma flow makes a transition from supersonic to subsonic flow in the spacecraft frame. This implied that high Mach number detectors optimized for the solar wind, such as Faraday cups, were less effective in separating the flow changes from the thermalization signatures and led to some ambiguities about the thickness of the shocks. By contrast interplanetary shock waves had been observed with Pioneer spacecraft free from this systematic problem since the shock and unshocked gas are both supersonic in the spacecraft frame. Early measurements could only resolve the components of the flow velocity in the spin plane of the spacecraft, if at all. Interplanetary missions rarely had sufficient time resolution to comment on the layer physics or the heating mechanisms. However, interplanetary shocks can be exploited, for example, to illustrate the true extent of quasi-parallel shock layers /7,8/. Voyager and ISEE data illustrated that the gas deceleration takes place at a narrow resolved layer on a scale much smaller than the spatial domain occupied by the precursors waves, thus refuting the early concepts of a multi-thousand ion inertial length quasi-parallel shock layer.

With the advent of the ISEE 1,2,3 and AMPTE-IRM data sets considerable new insights have been obtained for the physics of shock heating. This review paper will concentrate on those aspects that pertain to the electrons, reviewing the observational relations that are now fairly securely established and the evolving theoretical picture that has emerged primarily in the last decade. In particular there is now a clear answer why the electrons get such a small fraction of the heating available, and there is a clear answer on the importance of microinstabilities within collisionless shocks layers. As is usually the case, the quasi-neutrality of the plasma strongly couples the ion and electron physics in the layer.

WEAK INTERPLANETARY SHOCKS

Surveys with ISEE-3 of the electron heating produced by interplanetary shocks yielded little information on their structure since these shocks are convected over the spacecraft by the supersonic solar wind. This situation should be contrasted with the same instrumentation that resolves the shock structure within the nearly standing bow shocks discussed below. However, some new information on the phase space partition of energy at small Mach numbers was obtained. The energy available is small and the electrons are observed to get some of the directed energy made available. Feldman and co-workers noted /9/ that the increase in dispersion of $f(\mathbf{v})$ transverse to the magnetic field seemed to be the principal response in the electrons to the passage of the shock, although one particularly strong interplanetary shock showed a pronounced increase in dispersion both along and transverse to the local magnetic field direction as well as a flat top. Since interplanetary shocks have a much larger radius of curvature than bow shocks, these rare observations suggested that flat-topped distributions do not owe their existence to the curvature of planetary bow shocks, but to the intrinsic strength of the shock.

The asymptotic jumps in temperature were modeled by an assumed polytrope relation based on the high (low) entropy side temperatures, $T_{H(L)}$, and densities $n_{H(L)}$. The polytrope has not been evaluated in any overdetermined sense *through* the shock layer, however. Substantial scatter is evident in the determinations with $\langle \gamma_{eff} \rangle \simeq 1.6$ estimated for weak interplanetary shocks.

Like the strong bow shock samples the interplanetary shocks suggested that the electron heating, $[T_e] \equiv T_{e,H} - T_{e,L}$, was (i) correlated with that of the ions, $[T_e]_{IPM} = \alpha[T_i]$, and (ii) were consistently weaker with $\alpha \simeq 0.14$. The overall magnitude of the interplanetary shock electron heating

$[T_e]$ was (iii) organized by the magnitude of the change in the solar wind flow speed across the shock. These three relations remain characteristic of electron heating at all fast mode shocks of all strengths /10,11/. For data sets biased by the preponderance of strong bow shock crossings, $\alpha \simeq 0.2$; the correlation with speed jump seen in the weak interplanetary shocks is now understood as the weak disturbance limit of a correlation with the change in the kinetic energy of the flow across the shock, viz.

$$[T_e] = \epsilon[U^2] \tag{1}$$

which for weak interplanetary shocks of disturbance speed δU riding on the faster background wind, U_{SW}, we can find by linearization

$$[U^2] = U_2^2 - U_1^2 = (U_{SW} + \delta U_1)^2 - (U_{SW} + \delta U_2)^2 \simeq 2U_{SW}[U] \, .$$

This correlation is not terribly revealing of a heating mechanism, except that when the reservoir for heating goes up, electrons get heated more.

STRONG FAST (BOW) SHOCKS

Observations with the co-orbital ISEE 1-2 satellite pair have concentrated on the layer physics at the earth's bow shock and the magnetopause. Since these layers reflect disturbances that propagate with speeds that match and oppose the fluid flow where they occur, they "stand still" for inspection. Early studies /12/ yielded determinations of scale length and normals for shocks using two spacecraft; the shock layers of this low Mach number collection were too broad, $L \simeq c/\omega_{pi}$, to yield the sizable drift rates required by fashionable instabilities of the ion-acoustic type. These studies signaled that all was not well with the old paradigm for collisionless shocks of even the weakest (subcritical) type, where resistivity was thought to be an adequate form of dissipation required for their existence.

New insight into the mechanism for shock heating and the details of the electron preheating can be found in survey work /13,14/ using ISEE 1 and 2 data. Because the solar wind electrons are subsonic, they sample the shock and return before the ions in the observer's volume element can do so. All manner of electron precursor effects have been found, including mirroring signatures from the upcoming magnetic ramp and energization signatures /15,16,17/. These effects and those found by others at higher energies are reviewed elsewhere in this symposium /18/. For the present discussion such signatures are indicative of electrons interacting with an obstacle of relatively smooth appearances in the sense of applicability of guiding center motion.

Detailed spectra through the shock layer, made available by faster detectors and higher telemetry rates, revealed more details on the formation of the previously known flat-topped distribution functions. A time series of isocontours of the electron distribution function from the GSFC ISEE-1 VES detector across a supercritical earth's bow shock is presented in Figure 2 /19/. Each inset is oriented with the magnetic field direction in the $\hat{x}$ direction. In each inset the electrons coming back from the shock layer are moving in the $-\hat{x}$ direction. Upstream (early panel inset numbers) the characteristic solar wind distribution with pronounced thermal-suprathermal contrast is seen with a cool, nearly Maxwellian thermal population indicated by the equispaced concentric circles at low speeds. As the magnetic ramp is approached, increasingly complex signatures of back-welling electrons are seen, including mirroring signatures (insets 29, 32, 35); with depth of penetration through the shock layer, the low-energy phase space density becomes increasingly flat, but with structures of considerable complexity on its perimeter. While flat tops were commonly found behind the earth's strong fast shock /3,4,14/, the isotropy of the velocity space mesa depended on the location of the spacecraft inside the curved shock; the mesa was pear shaped, pointing in the direction *opposite* to the closest penetration of the shock along the local magnetosheath magnetic field line. Sometimes the flat-top mesa was concave in a caldera form; quite frequently there was a departure from the flat mesa on its high-energy extremity that was dubbed a "beam" as in Figure 3 /13/. This departure from the flat, mesa-like, appearance at low energy was usually seen near the sheath-ward edge of velocity space along **B** and was seen originally by Montgomery and collaborators /3/. The energy of this "beam" was monitored in some cases to increase with penetration into the shock layer, while

the amplitude of the beam was observed to diminish. The detection of this beam was interpreted to be the free energy for the subsequent instability rearrangement for broadening of the electron distribution function (/14/, p. 108). Possible instabilities in the presence of such beams also have been modeled /20/. The clear thrust was still in the Sagdeev paradigm: find the free energy to disperse by microinstabilities to do the heating. The beam formation was suggested to reflect the coherent shock electric and magnetic forces seen by the electron; however, no detailed phase space comparisons were performed to independently substantiate this association.

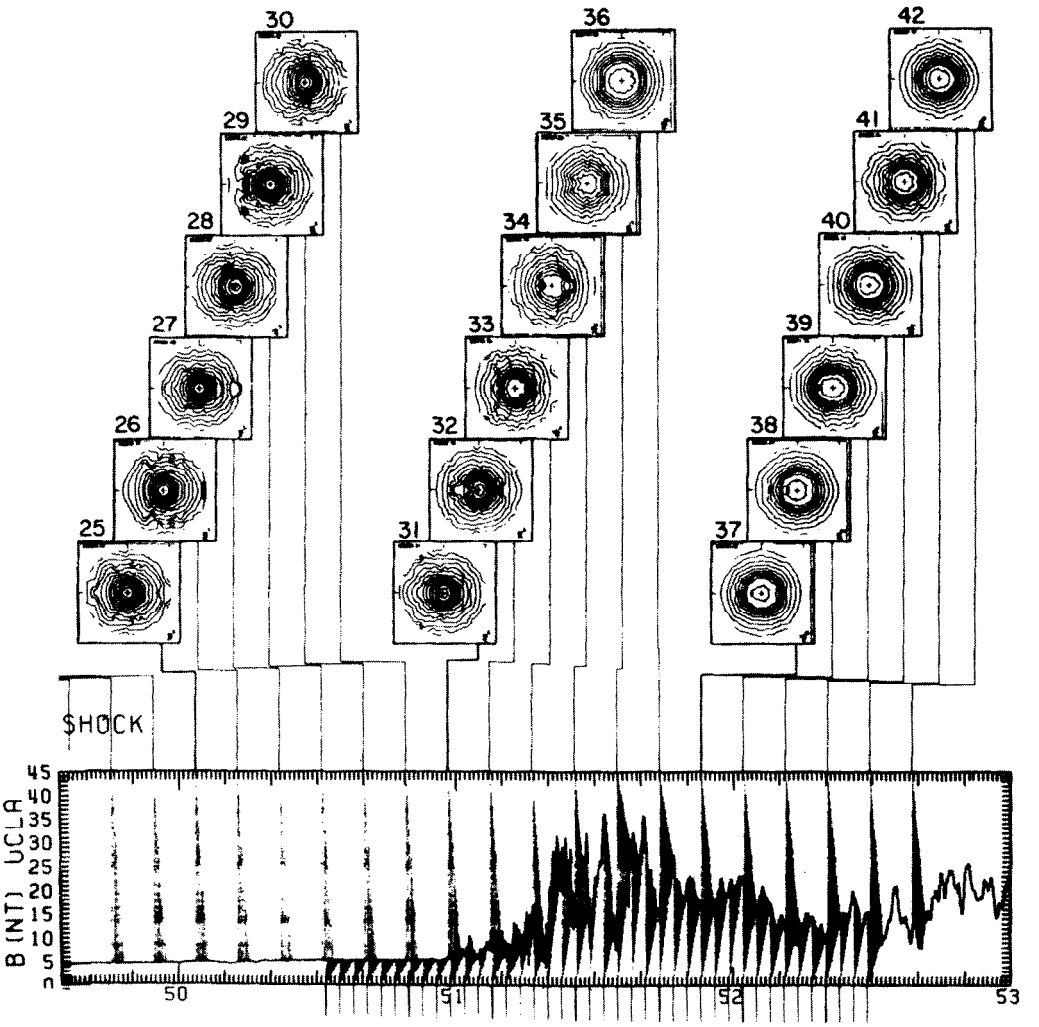

Fig. 2. Electron isocontour plots across a supercritical bow shock: ISEE 1 /19/. The magnetic field direction is always along the positive x axis in each inset box. The logarithm of the electron distribution function is contoured in equispaced levels in a $v_{\parallel}, v_{\perp}$ space in the center-of-mass frame. The magnetic intensity through the shock layer is indicated below, as well as the averaging-time interval which refers to the distribution functions.

However, the size of the work done by the electric force estimated from conservation equations was found to be four times *larger* than the observed kinetic energy of the beam. The authors surmised that the fluctuations of **B** within the quasi-perpendicular shock layer could in some way interdict the energization that *the* DC electric field would otherwise have given to the electrons. The difference between the applied potential and the observed beam energy was presumed to have had been deposited in some other plasma form, presumably by instabilities tapping this new free energy. Beam modes were found /20/, but the instability analysis was performed on the observed time-

aliased distributions, not those free-streaming distributions in an accelerating potential four times the beam energy.

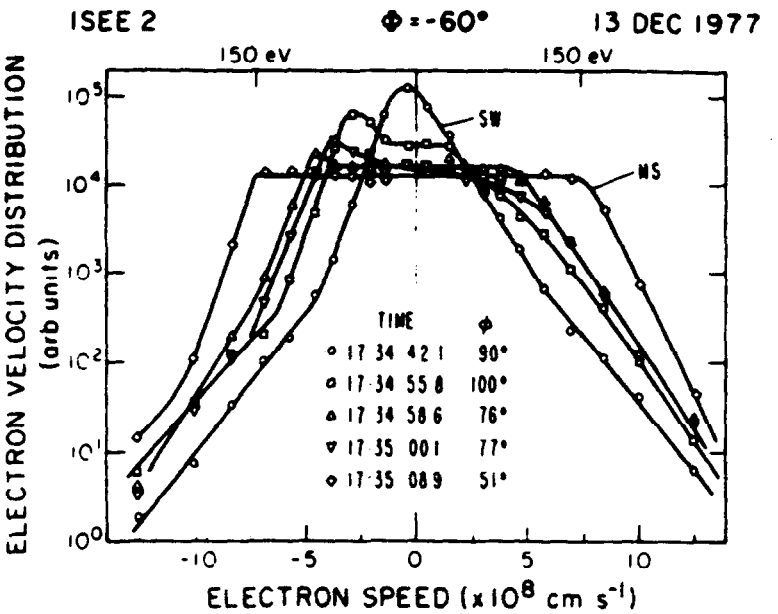

Fig. 3. "Beams" on the magnetosheath toward edge (at negative "speeds") of the flat-topped distribution as a sequence through the shock layer /13,14/.

The Relevant Cross Shock Electric Field for Electrons

In 1982 one of the coauthors of the early ISEE papers /13,14/ focused the community's attention on the discrepancy between the solar wind ion's loss of kinetic energy to electrical potential energy across the quasi-perpendicular supercritical shock on the one hand, and the much smaller observed energy gain of the electrons from the same electric field on the other. The estimated coherent electric force in the shock for electrons /13,14/, was four times that necessary to explain the kinetic energy of the electron beams. In this time frame the role of an electric field along the shock normal, although known from laboratory shock work, was demonstrated to play an important role in explaining the observed ion dynamics /21/. The electron experimenters /13,14/ estimated *the* size of *the* cross shock potential using

$$e\Delta\Phi'(x) \simeq \int_{-\infty}^{x} \frac{1}{n(x')} \frac{d}{dx'} \left[\frac{B(x')^2}{8\pi} + n(x')kT(x') \right] dx' , \qquad (2)$$

where x', as in the customary NI frame defined in Goodrich and Scudder /1/, is the distance along the shock normal, the asymptotic field and flow are in the (x-z) plane and the cross field ramp current flow of the fast mode shock is in the $-\hat{y}$ direction. For a supercritical perpendicular shock the potential given by (2) is *everywhere less* than the complete expression for this potential /21,22/ for the NI electric field when the (gyrating) ion's y velocity contribution to E_x is considered, viz.

$$e\Delta\Phi(x) \simeq \int_{-\infty}^{x} \frac{1}{n(x')} \frac{d}{dx'} \left[\frac{B(x')^2}{8\pi} + n(x')kT(x') \right] dx' + \frac{1}{c} \int_{-\infty}^{x} V_{yi}(x')B_z(x')dx' . \qquad (3)$$

The contrast between these two potentials is illustrated in Figure 4 from /21/ and is related to the ion's bulk motion perpendicular to the coplanarity plane, V_{yi}, that introduces a new scale to the potential formation, namely the convected ion inertial length, $CIIL_2 \equiv V_{x1}/\Omega_{ci2}$. Thus the omitted term of (3) from (2) doubles the electron experimenters' published disparity between emf and beam kinetic energy and calls into question the role of the electric emf in the formation of the beam, since a more complete estimate makes the $\Delta\Phi$ of this example eight times the measured electron beam kinetic energy.

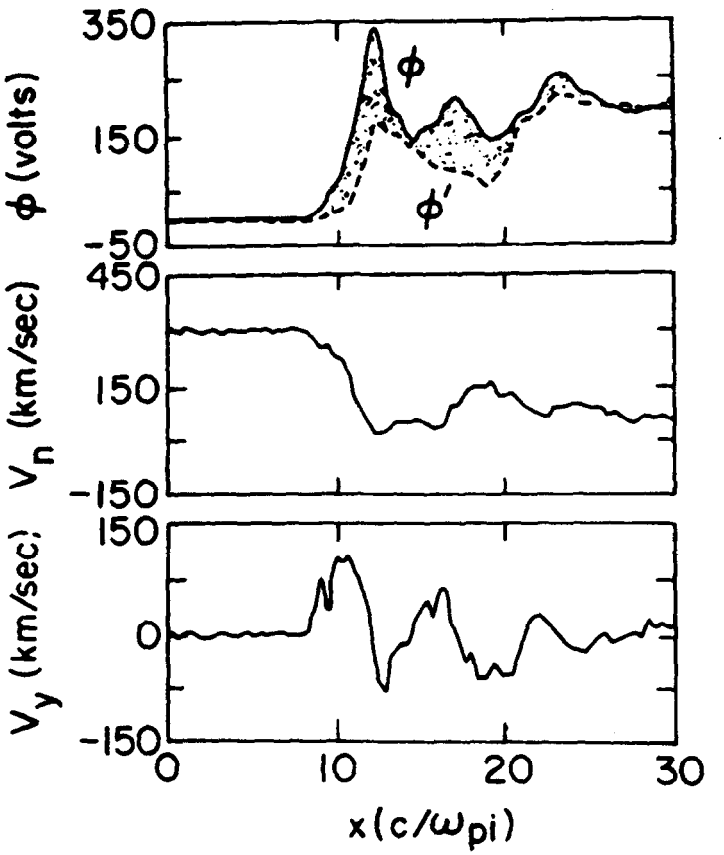

Fig. 4. $\Phi(x), \Phi'(x)$: NI Potential Profiles with and without gyrating ion contributions /21,22/. Early electron interpretations used Φ' to compare with the electron beam energies as illustrated in Figure 3. This Φ' was already four times the observed beam kinetic energies. The actual potentials that should have been compared were those of Φ, making the energetics even more bewildering. For future reference notice the scale of the NI potential across the shock, extending into the pedestal and behind the ramp for scale lengths of order c/ω_{pi}. Compare with Figure 7b where observations illustrate a similar broad potential distribution across the shock layer.

Retreating a moment, the traditional shock frames should be defined. The so-called NI frame /1/ is that shock frame where the shock layer is at rest and the bulk velocity vector, $\mathbf{U}_L$, on the low-entropy side of the shock approaches the shock along the local shock normal, $\hat{\mathbf{n}}$. The low-entropy side magnetic field $\mathbf{B}_L$, this flow vector and the shock normal define a coplanarity plane which, in turn, is parallel to another plane defined by the high-entropy flow, $\mathbf{U}_H$, the magnetic field, $\mathbf{B}_H$, and normal directions. The HT frame is that special shock rest frame where the *asymptotic* fluid and the magnetic field on *both* sides of the shock layer are aligned. The HT frame is attainable from the NI frame by a Galilean transformation that slides *along* the shock surface in a coplanarity plane so that the incoming flow appears to be aligned with $\mathbf{B}$. In this frame (i) there is no component of $\mathbf{E}$ tangential to the plane of the shock, (ii) there is no Poynting flux into the rearrangement of the energy of the plasma at the layer, and (iii) there is only a possible energy exchange between the plasma constituents between their directed and nondirected energies. For a 400km/s solar wind and shock normal $\Theta_{Bn1} \leq 88°$, the required transformation is a nonrelativistic transformation. Unfortunately for the electron experimentalists, the contemporaneous simulations were of perpendicular shocks done in the NI frame rather than the unattainable HT frame.

Goodrich and Scudder (GS) /1/ and subsequent experimental work /19,23,24/ resolved the electron heating quandary posed by the initial beam reports /13,14/. GS /1/ argued that with their smaller mass the electrons are more appropriately idealized as magnetized than the ions. Thus, their net

energization in the NI frame, unlike the ion loss of directed energy, is not so easy to foresee since the electron trajectories as a group are different in the shock (x-y) plane than the nearly rectilinear ions. The electron and ion energy changes are related to the *number of electrical equipotentials traversed*. In the traditional (NI) simulation coordinate systems, there is a tangential electric field in the plane of the shock layer perpendicular to the low-entropy coplanarity plane. This is an MHD electric field caused by the impinging magnetized plasma. From this fact it is clear that the NI electrical potential $\Phi^{\rm NI}(x,y)$ depends on both the coordinate along the normal, x, and that perpendicular to the coplanarity plane, y. Within the shock layer proper there is also a component of the electric field along the shock normal that has a primary sense to slow ions and is localized *within* the shock transition. Figure 5a from GS illustrates the topology of the electrical potential in the (x-y) plane in the NI frame. Also illustrated are the crude average paths of the ion and electron flow lines through the shock. Figure 5b illustrates the topology of the electric equipotentials in the HT frame. Because the electrons are more magnetized than the ions, they successfully $\mathbf{E} \times \mathbf{B}$ drift in the $\hat{y}$ direction, thereby moving more nearly along the NI electrical equipotentials. The nearly unmagnetized ions hurdle the thin layer, jumping almost all the equipotentials. *The different average interactions of the electron and ion fluids with the same electric field structure stems from the different paths that their average flow lines take across the equipotential structure; these distinctions all stem from the disparate electron and ion inertia. This recurring point in shock physics gets rediscovered every few years.*

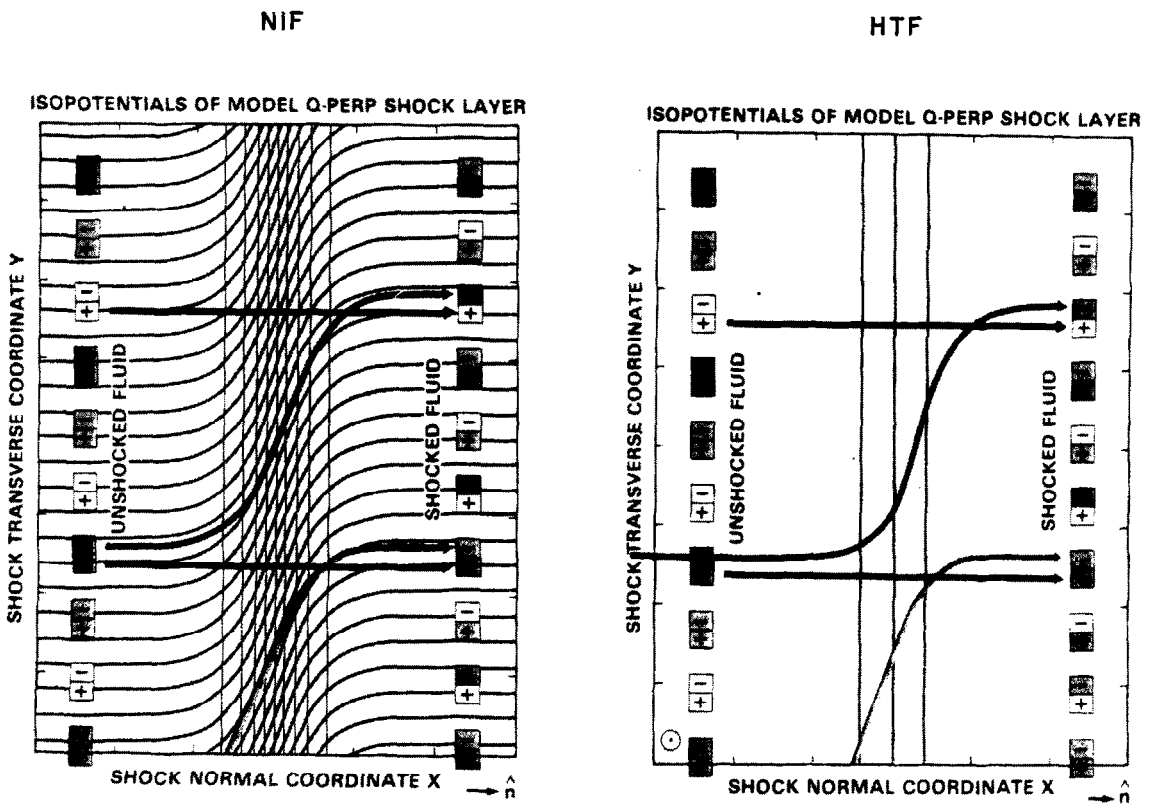

Fig. 5. Electrical potential topology in the x-y plane at shock (a) in the NI and (b) in the HT frame. Gross location of ion and electron flow lines in the x-z plane *resulting from the nearly complete magnetization of the electrons in contrast with the ions—a consequence of their disparate mass* /1/.

The usefulness of the NI frame is that its cross shock potential along the normal is $\simeq 80\%$ of the energy given up by the ion bulk flow as it traverses the layer. The bookkeeping of the residual number of equipotentials traversed by electrons and hence their *energization* is most easily done by exploiting the small electron mass once again.

The electron energetics are most straightforward in the HT frame which only has an electric field component along the shock normal (cf. Figure 5b). Hence the HT electrical potential, $\Phi^{HT}(x)$, depends only on the spatial component along the shock normal in contrast with $\Phi^{NI}(x,y)$. Because of the small electron mass, and the small value of the frame transformation speed between NI and the HT, Goodrich and Scudder /1,25/ argued that the observed energy gain $\Delta\zeta_e$ of electrons in the spacecraft, the NI or the HT frame is *essentially* the same and for all practical purposes indistinguishable, though formally different.

Figure 6 illustrates /25/ the *difference* between the NI and HT frames of the *energy change*, $\Delta\zeta_e$, across the shock as a function of Θ_{Bn1} and the Alfvén Mach number, M_A, derived by Goodrich and Scudder /1/, who explicitly used the asymptotic zero current condition, $[V_{ze}] = [V_{zi}]$. An upper bound for this slight difference is 0.05 eV, a nonzero effect, but utterly negligible at 1 AU (cf. exchange between /26/ and /25/). *Thus, if the* HT *frame is accessible for the shock geometry in hand, the* HT *frame observer's determination of the energy available should suffice for all practical purposes for all shock frame observers.* This being the case, the energy gain for electrons in the HT frame is conceptually easier to visualize, since the electric field in this frame only exists along the shock normal. If the electron gets across the layer, then its energy can only change by the HT electrical potential jump, which as GS argued *can* be different from the (NI) electrical potential jump estimated by Feldman and coworkers. In particular, GS reasoned for fast shocks that if the internal layer of the shock had a positive mean value of B_y/B_x, then the disparity of energetics for ion deceleration and electron gain would be resolved.

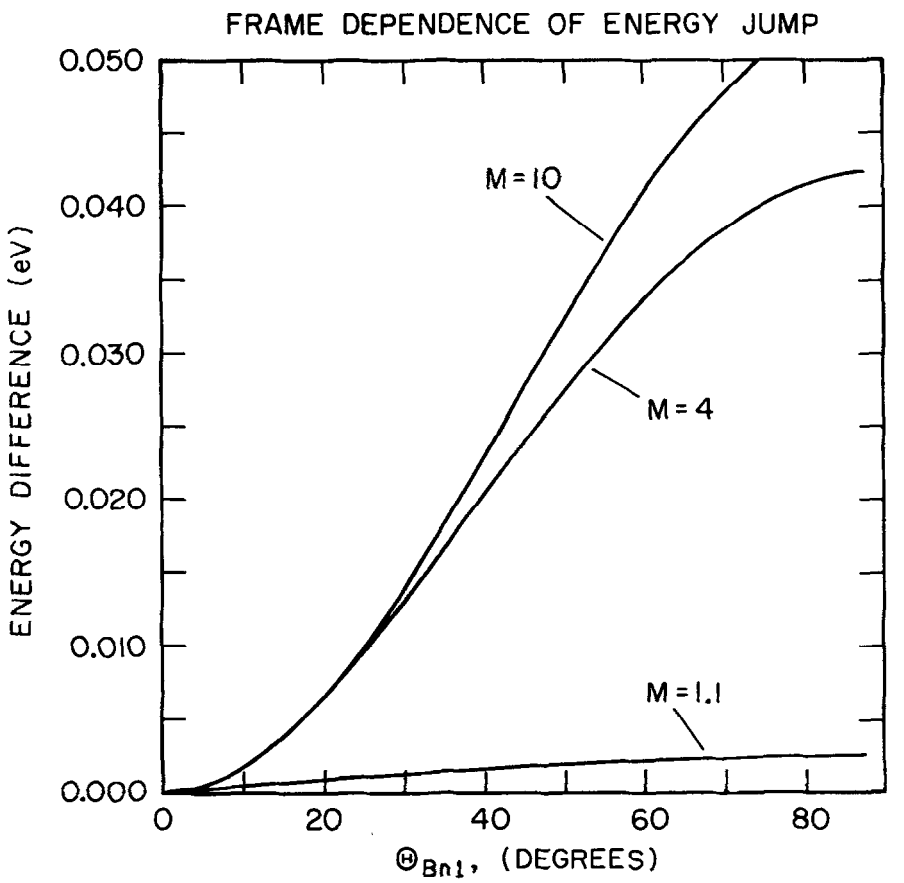

Fig. 6. Difference in the change in electron energy between the NI and HT frames for Θ_{Bn1} and M_A /25/. Notice that the frame dependence of the energy changes is small compared to 1 AU thermal spreads of 10 eV.

This may be seen since the electric field in these two frames are related by special relativity. The HT observer slides along the shock front as viewed in the NI frame with a velocity given by

$$\mathbf{V}^{\mathrm{HT}} = -c\,\frac{|\mathbf{E_T}|}{B_x}\,\hat{\mathbf{z}}\,. \tag{4}$$

The HT observer records a weakened electric field with only an x component:

$$\mathbf{E}_x^{\mathrm{HT}} = \mathbf{E}_x^{\mathrm{NI}} + \frac{|\mathbf{E}_T|}{B_x}\,\mathbf{B}_y(x)\,, \tag{5}$$

where it should be noted that $E_x^{\mathrm{NI}} < 0$. This condition determines a relation between two different potential jumps in the two frames for a common path that goes along the shock normal from the low- to high-entropy side, viz.:

$$\Delta\Phi^{\mathrm{HT}} = \Delta\Phi^{\mathrm{NI}} - |\mathbf{E}_T| \int_0^{\Delta x} \frac{B_y(x')}{B_x}\,dx'\,. \tag{6}$$

Note that any path across the shock from low- to high-entropy side in the HT frame gives the same potential drop as that along the normal; this is not the case in the NI frame. The electron motion in the HT frame in the (x-y) plane is identical to that in the NI frame. Its line integral across the layer in the HT frame is the same whether there is a drift in the $\hat{\mathbf{y}}$ direction or not.

The integral of (2) approximated by Feldman and coworkers /13,14/ is a lower bound for the NI potential, (3), the electrical potential change experienced by a supersonic *ion* in the NI frame, $\Delta\Phi^{\mathrm{NI}}$, as it "hurdles" the current-carrying ramp, moving essentially along the shock normal. However the electron gets across the layer in the HT frame, it gains the potential energy associated with superscript "HT." But since the energy gain *for electrons* is **almost** independent of frame, this should be the observed potential jump embedded in the electron heating observations in the spacecraft frame of reference. The innocuous integral in (6) *over the magnetic substructure of the shock* defines a length, viz.

$$[R_{yB}] \equiv \int_0^{\Delta x} \frac{B_y(x')}{B_x}\,dx', \tag{7}$$

that was suggested /1/ to be a positive quantity for fast mode shocks to explain this disparity between what kinetic energy that the transmitted solar wind ion beam lost and the electrons gained in the fast mode bow shock. The existence, however, of $B_y(x)$ throughout the layer was not a novel concept to the GS paper, but had been summarized more than a decade earlier in Tidman and Krall's classic monograph /27/ and cited by GS (/1/, p. 6655).

The leverage for the suggestion of GS that $[R_{yB}]_{\mathrm{fast}} > 0$ becomes available **only** with the introduction of new information about the scale lengths of observed shocks and their relation to those scales of electrons and ions. It is not a consequence of the one-fluid conservation laws summarized by the Hugoniot relations. *It should not, therefore, be surprising that the ab initio evaluation of this integral* **cannot** *be determined in closed form from the one-fluid state variables that are the asymptotic states required by boundary conditions.* This last statement is made notwithstanding the erroneous, "first principle" derivations to this effect published in the literature and discussed below.

GS also reconciled the description of the same electron behavior as viewed in the NI and HT frames /1/. They illustrated that the guiding center motion of the electrons in the NI frame in the layer caused them simultaneously to be accelerated toward the shocked gas and along the shock surface. Unlike the HT frame, the NI frame has a tangential electric field along the shock surface, *and* the $\mathbf{E}_x \times \mathbf{B}$ drift of the electrons pushes them to do work along the $\mathbf{E_T}$, causing the electron gas to give up a significant fraction of the energy that they had gained by making progress along the normal. That is the essential tension of the two terms on the right-hand side of equation (6).

GS gave a closed form solution for the electric field in the HT frame that was independent of the NI frame electric field, demonstrating that this electric field was just the electric field required to ensure quasi-neutrality in the shock layer. This derivation was possible since $\mathbf{E}^{\mathrm{HT}}$ only has an x component, because $\mathbf{E} \cdot \mathbf{B}$ is a relativistic frame invariant, and because $|\mathbf{B}|$ is a nonrelativistic invariant. Manipulating the electron momentum equation, the approximate form presented by GS neglected electron inertia and resistivity

$$\mathbf{E}^{\mathrm{HT}} = -\frac{\nabla \cdot \mathbf{P}_e}{en_e} + \mathrm{H.O.T.} \tag{8}$$

and is clearly to be identified with the ambipolar electric field. The general frame invariant expression /23,28/ involves the acceleration of the center of mass of the electrons, the parallel resistivity, and the spatial variation of the anisotropic pressure of the electron which if the electrons remain magnetized (and P then gyrotropic), takes on the form:

$$\mathbf{E}^{\mathrm{HT}} = \left\{ -\frac{1}{en_e}\left(\frac{dP_{\parallel,e}}{dx} - \left(P_{\parallel,e} - P_{\perp,e}\right) \frac{d\ln B}{dx} \right) - \frac{mV_{xe}}{\hat{\mathbf{b}} \cdot \hat{x}}\, \hat{\mathbf{b}} \cdot \frac{d\mathbf{V}_e}{dx} + \frac{\eta_{\parallel} J_{\parallel}}{\hat{b} \cdot \hat{x}} \right\} \hat{\mathbf{x}}\,, \tag{9}$$

where $\eta_{\parallel}$ is the parallel resistivity.

To make their point that $[\Phi^{\mathrm{HT}}] \ll [\Phi^{\mathrm{NI}}]$, GS *estimated* the change in this potential under the previously modeled isotropic polytrope modeling of electron heating, viz.

$$|e|[\Phi^{\mathrm{HT}}] \simeq \frac{\gamma_e}{\gamma_e - 1}\,[kT_e]\,, \tag{10}$$

and contrasted this with the much larger estimates of the

$$[e\Phi^{\mathrm{NI}}] \simeq -\zeta\,[\tfrac{1}{2}\,MU_n^2]\,, \tag{11}$$

the latter approximation consistent with simulations and observations with $\zeta(M_A = 6) \simeq 0.7$ /21/.

The extensively documented quasi-perpendicular supercritical shock reported by Scudder and coauthors /19,23,24/ has played a crucial rule in making the theoretical distinctions of GS concrete by providing empirical examples of the difference of the electric fields and their effects. This study remains to date the *only* shock for which $\Phi^{\mathrm{HT}}(x)$ has been determined by direct quadrature of (9) with all anisotropy (rather than 10). Similarly, this is the only experimental work where $\Phi^{\mathrm{NI}}(x)$ is also directly determined from the plasma observables and the normal momentum equation and compared with the electric double probe data through the layer as well as the proxy ion bulk deceleration. In this well-studied example the ratio of the two cross shock potentials is known fairly accurately to be $[\Phi^{\mathrm{HT}}]/[\Phi^{\mathrm{NI}}] \simeq 0.1$. The empirically derived potential profiles are contrasted in Figure 7a revealing an overshoot in the NI and HT potential profiles; the magnetic intensity profile through the shock is also plotted for the reference of structures in the electric field to those in the magnetic profile. Figure 7b shows the empirical $\Phi(x,0)^{\mathrm{NI}}$ for the purpose of showing that *the total* NI *jump occurs across a larger* $CIIL_2$ *scale*, $\simeq$ 175 km, *than that of the magnetic ramp*, $\simeq$ 14 km. The scale of the NI potential jump reaches out into the pedestal and well back into the magnetic overshoot. This scaling is in good agreement with the hybrid simulations (cf. Figure 4 above). The NI electric field within the magnetic ramp is considerably smaller than one would estimate by putting the entire inferred 410 V drop across the 14 km magnetic ramp.

The Ohm's law determination /23/ of E_x^{NI} was compared with that from the direct measurements from the double probes on the same spacecraft. The dominant components of the $\mathbf{E} \times \mathbf{B}$ were determined from the field measurements and the particles. The are favorably compared in Figure 8. Independent estimates of the (NI) electric field at other shocks by double probe electric field measurements have also been reported /28/. Both of these fast mode shock studies showed by the relativity transformation /5/ that the observed NI frame electric field along the normal was substantially reduced for the HT frame observer as suggested by GS. For the weaker HT electric

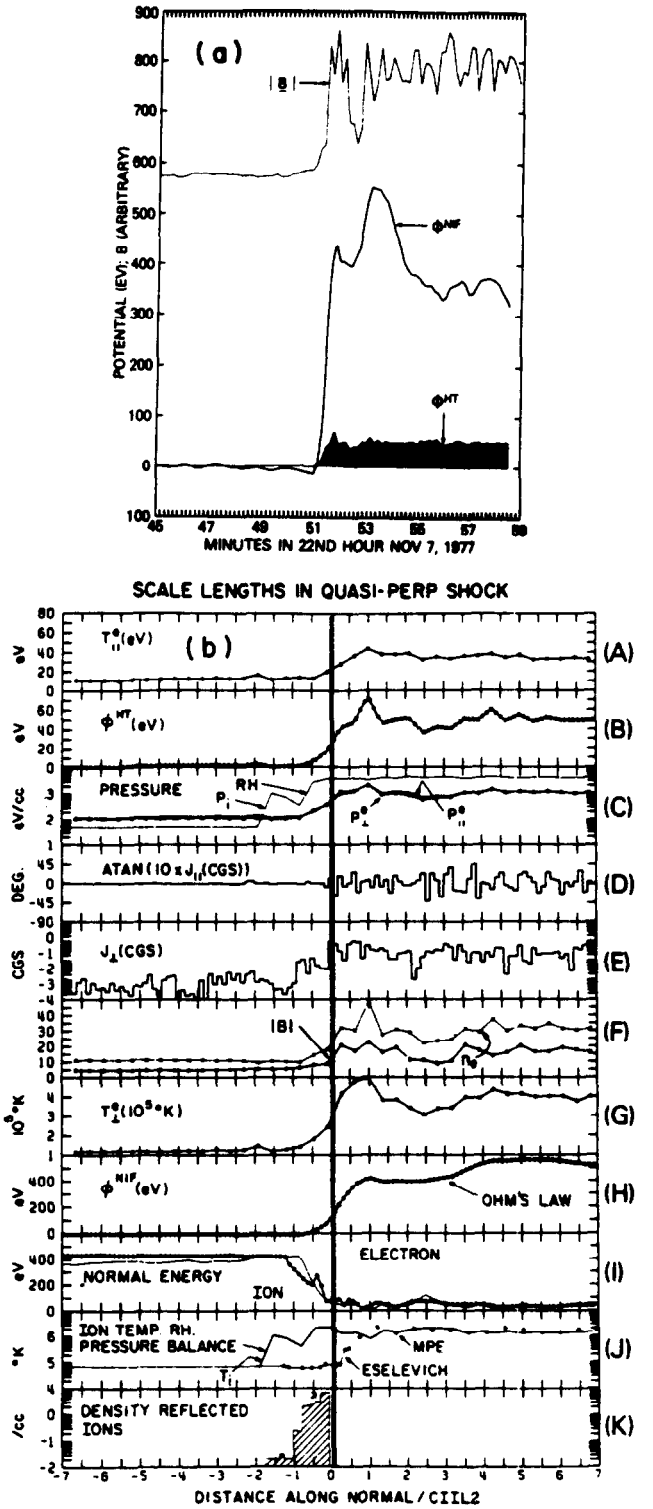

Fig. 7. (a) Observed NI and HT potentials determined /23/ from the generalized Ohm's law and electron observations that resolve the shock layer, with B in background vs time; (b) subset of observed field and plasma variables—including the NI Φ^{NI} and HT Φ^{HT}—across the same shock vs space. Note the close correlation of $T_{\parallel,e}$ and $[\Phi^{HT}]$ and $T_{\perp,e}$ with $|B|$ in cosets A,B and F,G, respectively. The magnetic ramp where the currents are most intense is localized between the two closely spaced vertical lines at 0 distance. Units of space are those of the downstream convected inertial length, CIIL2.

fields the plasma determination using the divergence of the pressure tensor is the more sensitive method, particularly when (9) is integrated across the layer.

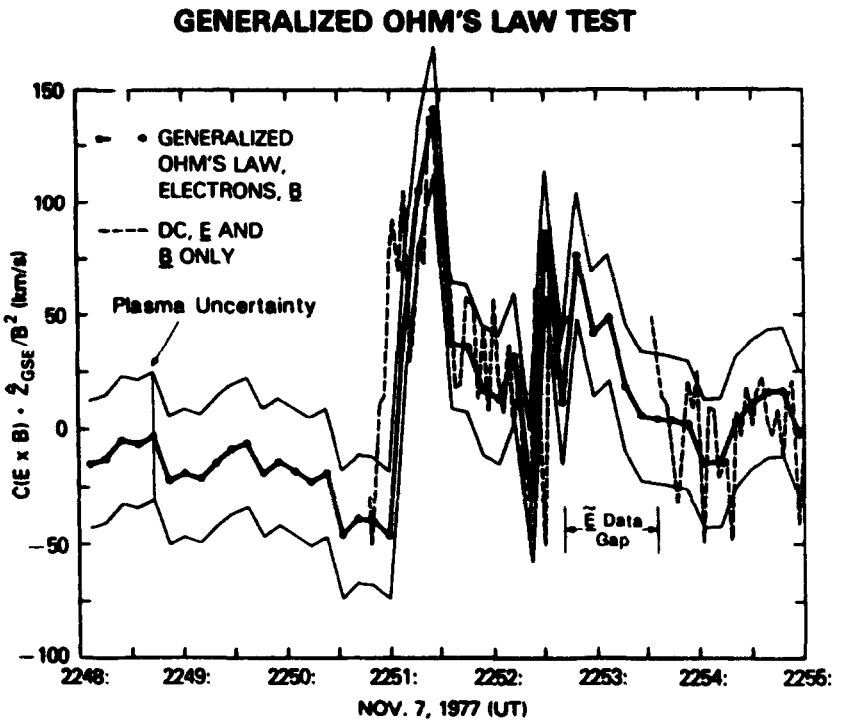

Fig. 8. $c(\mathbf{E} \times \mathbf{B}) \cdot \hat{z}/B^2$ drifts determined from $\mathbf{E}$ and $\mathbf{B}$ measurements and electron measurements through supercritical shock /23/.

Empirically it was also noticed /24/ that the increments of the HT frame electrical potential energy available to electrons were closely correlated with the incremental change in the magnitude of $|\mathbf{B}|$. This is actually a fairly general result noticed /30/ initially in the auroral context and then subsequently generalized /31/ for hot plasma.

In retrospect the distinction between the relevance of the NI and HT potentials was the missing ingredient in the Feldman and coworkers discussion /13,14/ of the cross shock energization as a coherent process. Had the HT potential been known then to be the relevant one, all the first-order electron morphology of the shock might have been viewed as a coherent process. Old paradigms change slowly, however, as evidenced by the instability scenario these authors advanced to explain the difference between the beam location and their incorrect estimates of the accelerating emf. Further, the moment heating of the electrons transverse to the magnetic field direction was viewed as a consequence of the redistribution of the energy difference into electrons, ions, and waves. By the time of his Chapman conference review /32/, Feldman had embraced the relevance of the HT frame field as the driving emf, but was still considering the relative importance of $\mathbf{E}^{HT}$ to the heating "... from conservation of magnetic moment and from cross field current driven instabilities [which] cannot be ruled out."

RELATIVE IMPORTANCE OF STOCHASTIC AND COHERENT "HEATING"

The realization that the coherent forces across the shock could produce almost all the observed increased dispersion of the electron distribution and, hence, its reported parallel and perpendicular temperature increase *without substantial instability mediation* was made clear by the detailed analysis of ISEE-1 and 2 data /19,23,24,33/. This analysis involved intracomparisons of data from ten investigations on the two spacecraft at a well-documented shock to illustrate that the electron phase space deformation *including its parallel and transverse dispersion* was quantitatively controlled by

space deformation *including its parallel and transverse dispersion* was quantitatively controlled by the simultaneously determined $\Phi^{HT}(x)$, from equation (9), and $B(x)$ profiles. These comparisons /24/ clearly showed the main deformation of the electron distribution, its enhanced dispersion or half-width, *throughout the resolved layer* was in *quantitative* response to the self-consistent, spatially varying, and nonmonotonic HT potential (Figure 7a) rather than the NI potential assumed previously /13,14/. The parallel electron temperature $[T_{\|,e}]$ of inset A of Figure 7b is closely governed by $[\Phi^{HT}]$ as illustrated in inset B of Figure 7b. Also note that $[T_{\perp,e}]$ follows [B] as illustrated in insets F,G of Figure 7b.

The same study /23/ demonstrated that the electrons at the local thermal speed were magnetized throughout the shock layer. This is illustrated in Figure 9 where the ratio of the scale length, L_B of changes in $|\mathbf{B}|$ are scaled by the local thermal electrons gyroradius, a_E. *Everywhere* within the shock layer this ratio exceeds 10 and more generally 100. These observations have been interpreted rather cavalierly by some /34/ seeking new heating mechanisms for shock waves like the bow shock.

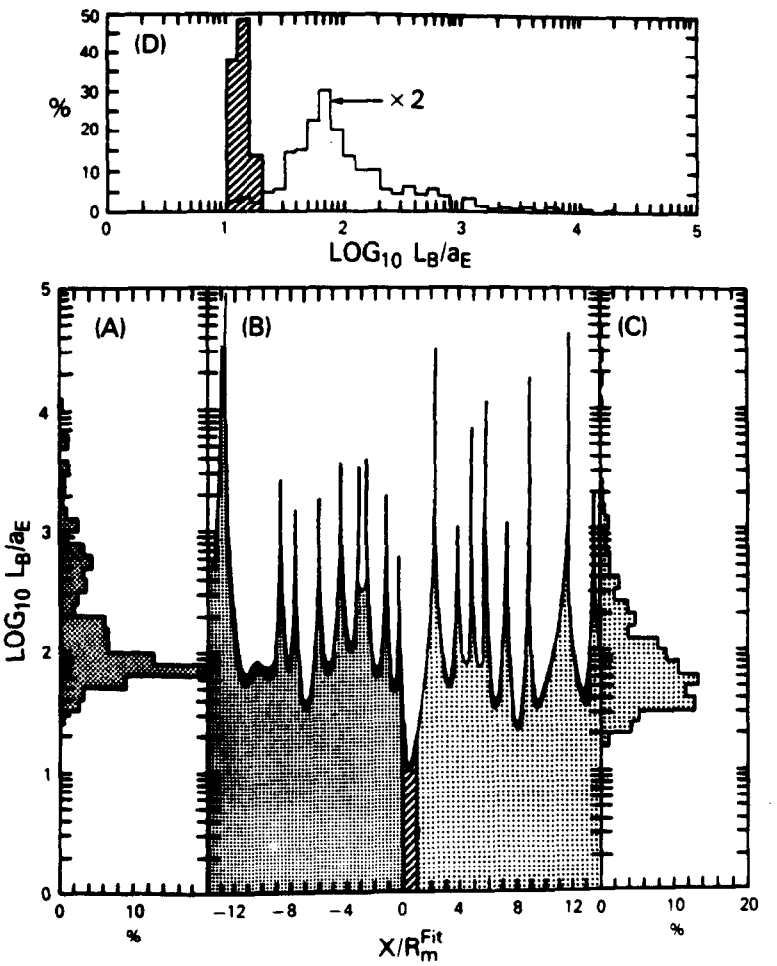

Fig. 9. Dimensionless gyroradius scales including demonstration of magnetization within the main magnetic ramp /23/. The scale length of B, L_B is determined by the logarithmic derivative, and the thermal gyroradius is denoted a_E. Panel (B) illustrates this ratio across the shock ramp. The spatial units of this survey are in units of the cross shock ramp thickness, R_M. Panels A and B represent histograms of the frequency of occurrence of varying dimensionless scales in upstream (A) and downstream regions (B). Panel (D) illustrates in the frequency distribution within the ramp proper, while the unshaded distribution reveals the composite frequency of occurrence distribution. This figure is shown to argue that the electrons should be modeled as magnetized throughout the layer.

The cross field drift is observed /19/ to be small and essentially that determined by $\mathbf{E} \times \mathbf{B}$ and is everywhere less than the electron thermal speed (cf. below where the contrary assumption is made). The cross field current from plasma measurements was determined for the first and only time to date /19/. The maximum ramp relative drift speed of 175 km/s was determined with a demonstrated signal-to-noise ratio of 6:1; it was well beneath the Galeev threshold necessary for ion-acoustic resistivity of 350 km/s. The implied current densities determined in this way were also corroborated by the two spacecraft thickness determinations of the main shock ramp. The traditional ion-acoustic instabilities were neither possible in this well-measured example, nor required to explain what was observed. The maximum measured or inferred electric field along the shock normal was 4 mV/m. This value should be contrasted with the assumptions made below of 30 mV/m /34/.

Assuming weak gradient guiding center behavior in the HT frame at a fast shock, it is easy to show that the Liouville streamed particles from the low-entropy side of the shock are found on the high-entropy side **outside** of a forbidden ellipsoid in velocity space given by the expression /35/

$$\frac{v_{\parallel,H}^2}{v_\phi^2} + \frac{v_{\perp,H}^2}{\frac{v_\phi^2 B_H}{[B]}} = 1 \,, \tag{12}$$

where $v_\phi^2 \equiv 2|e[\Phi^{HT}]|/m$. From this expression it is clear that this cavity is always preferentially elongated in the perpendicular direction. The ratio of the perpendicular (semimajor) axis, $a_\perp$, to the parallel (semiminor) axis, $a_\parallel$ is given by

$$\frac{a_\perp}{a_\parallel} = \left(\frac{B_H}{[B]}\right)^{1/2} \,, \tag{13}$$

being more elongated transverse to $\mathbf{B}$ than along it regardless of the size of $[\Delta\Phi^{HT}]$. Figure 10a,b illustrates the consequences of the shaping factors of this exclusion void for the high-entropy electron distribution across weak $B_H/B_L = 1.3$ and strong $B_H/B_L = 3.9$ shocks. In addition to this asymmetric inflation of the phase space, the overall radius of the inflation along $\mathbf{B}$ is controlled by the size of the HT potential which is directly related to shock strength. The excluded volume in phase space, which is a measure of the overall inflation induced in the electrons, is given by the expression

$$\text{Volume}_{\text{excluded}} = \frac{4}{3}\pi \frac{B_H}{[B]} v_\phi^3 \,.$$

This overall volume enhancement of the mapped phase space is illustrated in Figure 11, where isocontours of $f(\mathbf{v})$'s for the low-entropy and high-entropy sides of a strong, fast mode shock are depicted. The nearly circular though elliptical void gives rise to an increased moment dispersion, or temperature, implied by guiding center behavior in the presence of $E_\parallel$ and $\hat{\mathbf{b}} \cdot \nabla |B|$. Because the electrons are moving into the shock, the displaced upstream distribution gets mapped preferentially forward to develop the field-aligned beam. This mapping in the HT potential explains much of the morphology within the shock layer initially reported /13,14/ including the *nearly* isotropic increase of the dispersion of f parallel and perpendicular to $\mathbf{B}$ for strong fast shocks. (For weaker interplanetary shocks this same but now asymmetric inflation of Figure 10a provides an explanation for the reported /9/ preferential increase of dispersion of f perpendicular to $\mathbf{B}$.) These effects can explain the most commonly observed aspects of electron heating at strong bow shocks /24,35/. The high-entropy moment temperature is of the form

$$kT_{\text{moment}} \equiv \frac{2}{3} \frac{\int_{\text{ellipsoid}(v,\theta,\phi,v_\phi)}^{\infty} f(\mathbf{v}) \frac{1}{2} m v^4 \, dv \sin\theta \, d\theta \, d\phi}{\int_{\text{ellipsoid}(v,\theta,\phi,v_\phi)}^{\infty} f(\mathbf{v}) v^2 \, dv \sin\theta \, d\theta \, d\phi} \,. \tag{14a}$$

The coherent modification of the upstream and sheath distributions in the coherent HT potential and magnetic fields were contrasted /24/ with the observed phase space densities across the potential rise through the layer into the magnetosheath. The structure of the observed $f(v_\parallel, v_\perp = 0)$

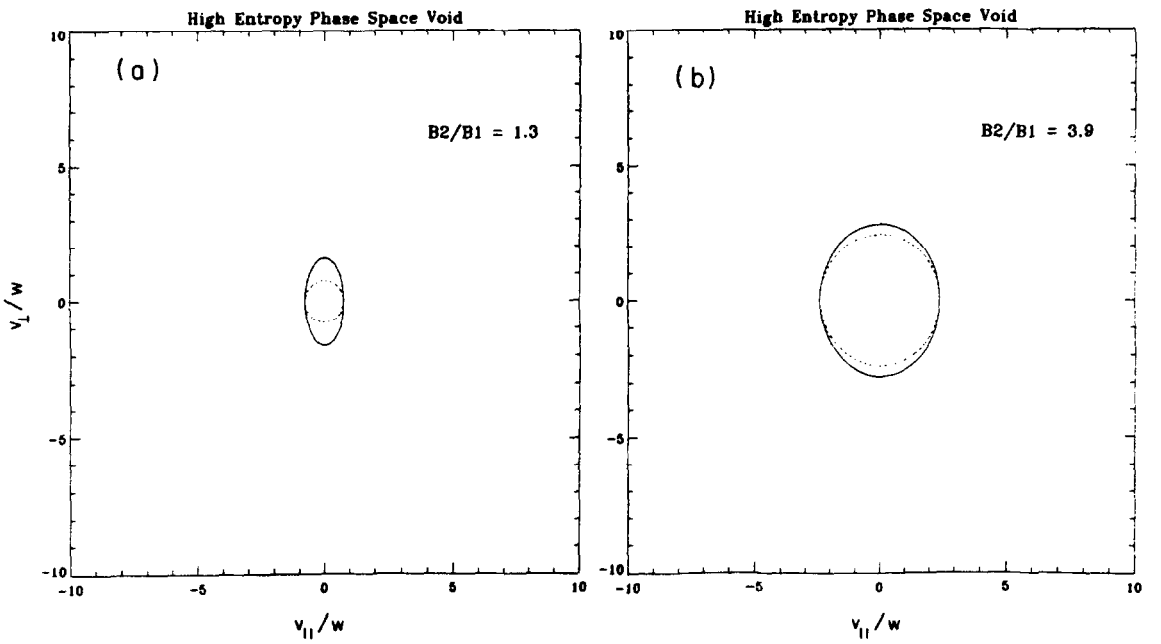

Fig. 10. Void ellipsoid for (a) Weak, (b) Strong fast magnetosonic shock /35/. The highly elliptical void would suggest preferential "inflation" in the transverse phase space of electrons at weaker (interplanetary) shocks as observed /19/ and more isotropic inflation at stronger shocks such as the earth's bow shock and stronger interplanetary bow shocks /14,24/.

was shown /24/ to respond to the spatially nonmonotonic features of the self-consistently determined HT potential profile of Figure 12. Inaccessible portions of phase space were identified and some of these regions were shown to be occupied, suggesting aspects of irreversibility. However, the overarchingly important conclusion was the dramatic coherent, DC, manipulation of the *perpendicular as well as parallel* temperature of the subsonic electrons caused by the DC accelerating field. This effect has been shown to be a general property of accelerating forces acting on a subsonic gas /36/. Occasionally erroneous arguments are published that $E_{||}$ gives preferential parallel temperature enhancements at shocks, and not the nearly isotropic heating observed. Figures 11 and 14a contradict this argument.

These data also showed (Figure 13) that the reported parallel dispersion increase of f, $\tau_{||}(x)$, that resulted from free-streaming solutions of Liouville in the HT forces at the shock provided *more than enough* dispersion to explain the temperature. The wave activity morphology and the quantitative followup /37/ demonstrated that the wave particle effects (recorded to be present and associated with the distinguishability of the reflected gyrating ions) weakly modify the dispersion of the electron distribution function. Some of these effects entail filling some of the Liouville induced voids (Figure 12), that emulate the "maximal trapping" procedure /38/ used by reference /24/ to slightly cool the Liouville deformed $f(\mathbf{v})$, in accord with the observed corresponding dispersion in the data. Also illustrated in /24/ were portions of phase space where modest wave particle enhancements in the suprathermals were observed; they, too, are relatively minor corrections to the effects of the HT potential.

Unlike the earlier paradigm whereby wave particle heating was thought to heat the gas (δE^2 is transferred to the kinetic motions of the particles), the observed relaxation from free streaming actually "cooled" the electron gas below its "reversible" inflation (illustrated in Figure 11) in the recorded HT potential. The maximal trapping operations on the Liouville streamed solutions were motivated by the observed $f(\mathbf{v})$ that clearly showed phase space density in locales where reversible theory in the coherent fields would suggest there should be none (as in the cross hatched voids of

Figures 10 and 11)—thus providing visible proof of a time-dependent prehistory and possibly the second-order smoothing role of microinstabilities.

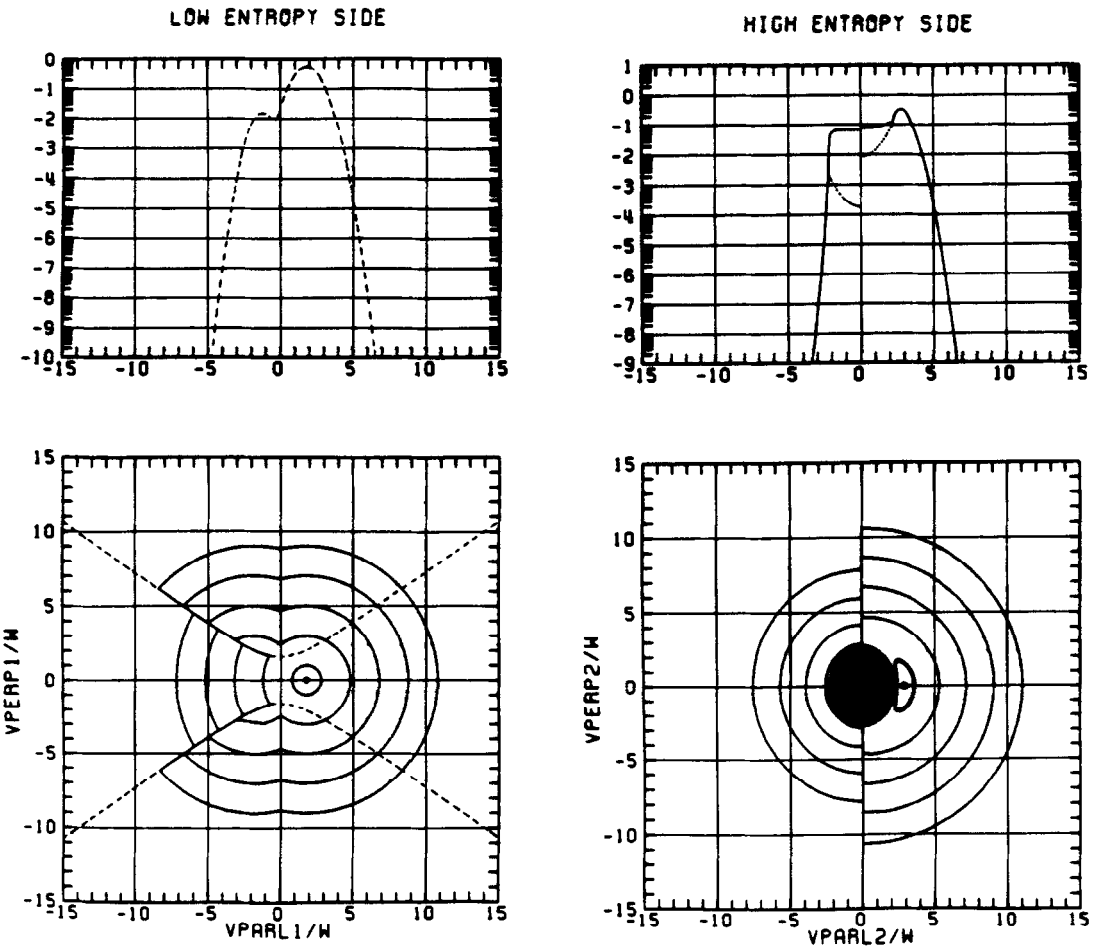

Fig. 11. Mapped $f(\mathbf{v},\mathbf{x})$ from (a) low-entropy side to (b) high-entropy side at a strong shock. Note the formation of the beam and the nearly symmetric overall inflation of phase space /24,35/.

The "cooling" property of waves is most easily seen by looking at the definition of a moment temperature

$$kT_{\text{moment}} \equiv \frac{2}{3}\frac{\int_0^\infty f(\mathbf{v})\,\frac{1}{2}\,mv^4\,dv\,\sin\theta\,d\theta\,d\phi}{\int_0^\infty f(\mathbf{v})v^2 dv\,\sin\theta\,d\theta\,d\phi}\,. \tag{14b}$$

The coherent forces produce a velocity space as the HT potential is traversed with an ellipsoidal void on the high-entropy side including the origin (illustrated in Figures 7b, 11b), while the upcoming magnetic field causes the reflected rays seen in the perturbed upstream solar wind as in Figure 11a. If the wave particle reactions rearrange the phase space density by taking some from the edge and top of the mesa and putting it in the void, the general effect is to increase the denominator of (14b) more than the numerator. This happens because near the origin in velocity space the integrand's contribution for flattening the plateau into the void grows like v^4, while the denominator grows like v^2. At the same time the removal of phase space density from higher-to-lower speeds penalizes the v^4 weighted numerator more than the v^2 weighted denominator. As can be seen in Figure 13 these trapping corrections, $(T^\tau \rightarrow T_\parallel^\xi)$, make rather modest "cooling" corrections to the lowest-order effects of the DC potential itself. Note the complete failure of CGL prediction for $T_\parallel$ in Figure 13.

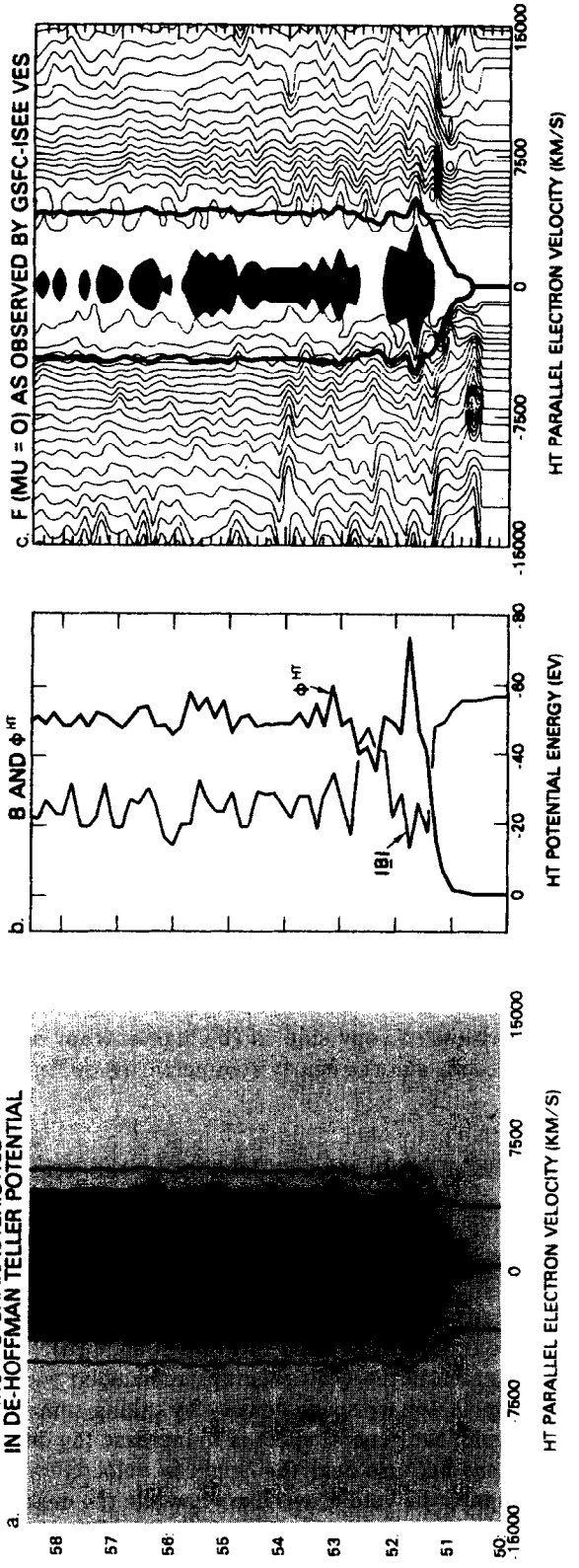

Fig. 12. Comparison of streamed $f(v_\parallel, \mu = 0, x)$ versus observations for parallel to B /24/. Leftmost panel indicates the topology of the characteristics. The heavy curve eminating from 0 velocity and then bifurcating at the shock is the separatrix for reversible trajectories determined by the solar wind distribution function. The solid curves outside this separatrix reflects a characteristic for the solar wind distribution. The dashed curve inside the separatrix reflects the characteristic for the sheath boundary conditions. The islands reflect reversible inaccessible domains of phase space. The middle panel illustrates the magnetic intensity and HT potential profile that determined the chracteristics in the left-most panel. The right-most panel is an isocontoure of the *observed* $\mu = 0$ electrons distribution function contoured over the transfered separatrix of the left-most panel. Note that the solar wind "information" is deformed to flow around the separatrix, although the mathematical contouring process has no knowledge of the separatrix boundary.

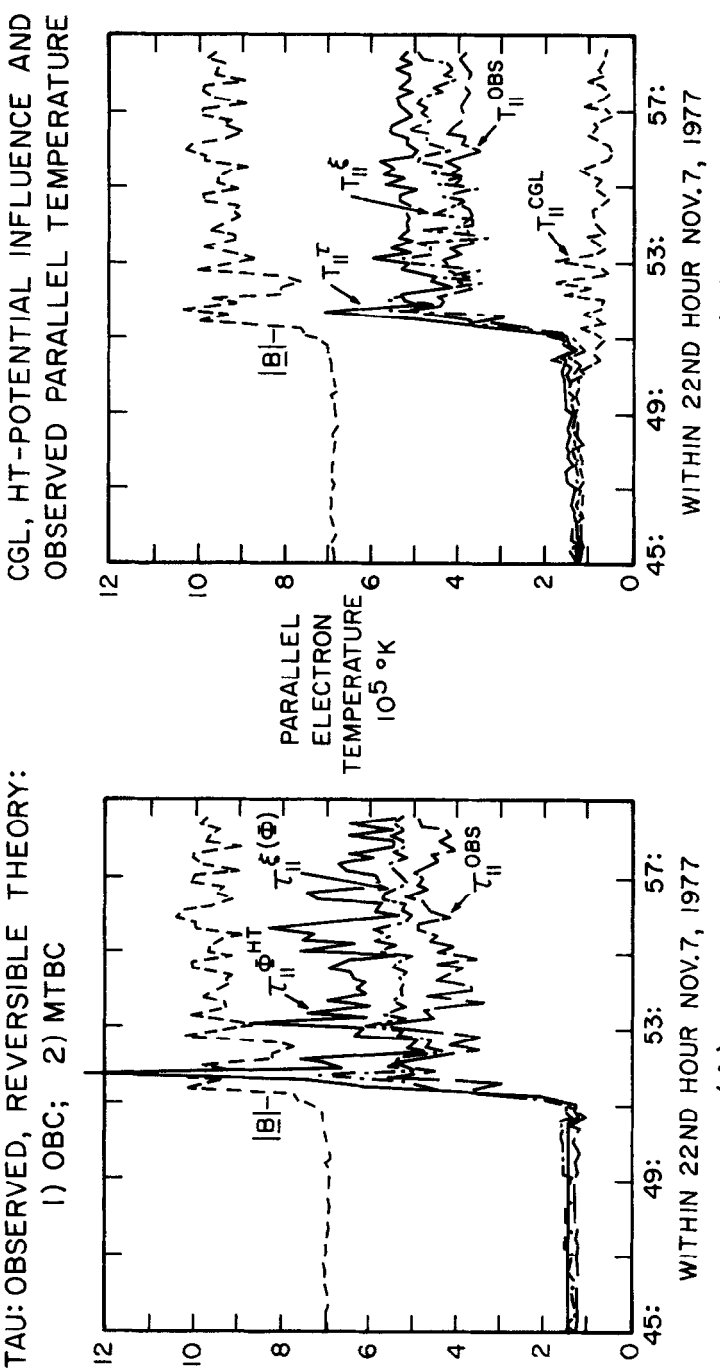

Fig. 13. Left panel: $\tau(x)$ profiles as the dispersion at zero pitch angle under three assumptions /24/: (i) reversible Vlasov, $\tau_{\|}^{\Phi^{HT}}$; (ii) maximal trapping recipe (cf /24/), $\tau_{\|}^{\xi(\Phi^{HT})}$; (iii) observed, $\tau_{\|}^{obs}$. Right panel: Various levels of $T_{\|}$ estimates based upon $T_{\|}$, ξ, and observed $T_{\|,e}$ as contrasted with CGL prediction.

The speed domain of the void, or its partially filled version in the caldera /14,24/ is theoretically controlled by the size of the HT potential drop /1,23/ and the change in magnetic intensity relative to the upstream region; the filling of this void is connected with meeting the requirements of quasineutrality /35/. At the same time the creation of this void by the DC forces pushes the mesa perimeter to higher speeds (cf. Figure 2 sequence across the shock) and increases the dispersion of $f(\mathbf{v})$, and hence causes the perpendicular and parallel "heating" deduced by the moments of the deformed distribution function. This is a coherent process.

A nonmonotonic polar integrated cut of a distribution function exhibited by Feldman and coauthors /13,14/ does not necessarily imply instability, even though it is called a "beam," a topic that excites instability experts. A search was performed using the fully three-dimensional GSFC VES electron spectrometer data through this shock for beams that were electrostatically unstable in the sense of Nyquist by computing the reduced distribution functions:

$$F(v_{\|}) = 2\pi \int_0^{\infty} f(\mathbf{v}) v_{\perp}\, dv_{\perp}.$$

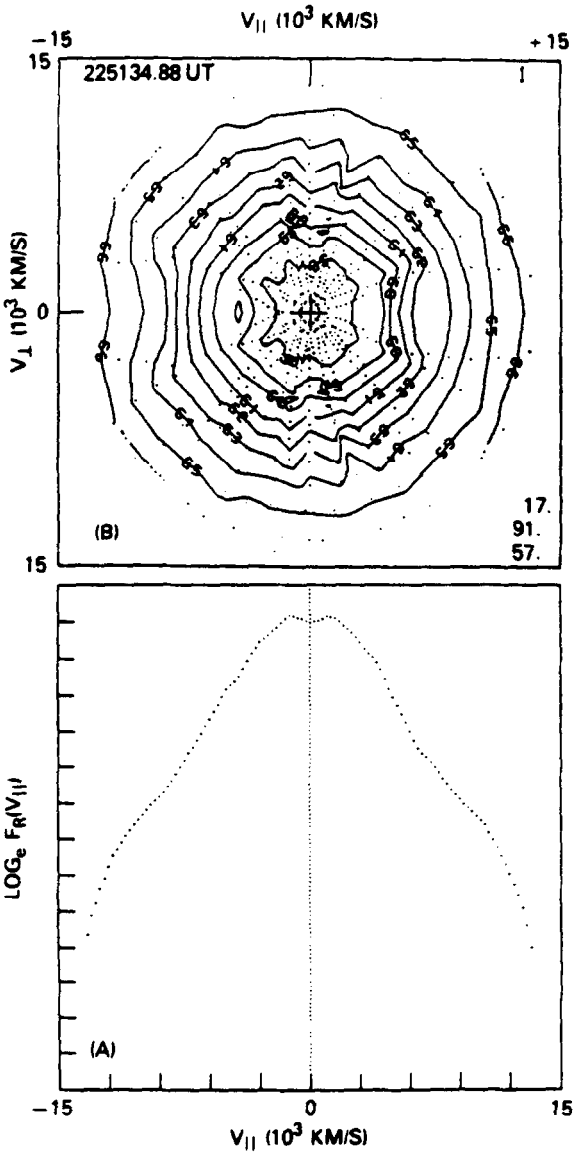

Fig. 14. Nyquist beam unstable distributions in middle of negative resistivity near overshoot of supercritical bow shock. Reduced distribution $F(v_{\|})$ in panel (A) and isocontour in the $v_{\|}, v_{\perp}$ plane of the logarithm of $f(\mathbf{v})$ that underlies it (panel B) /24/.

The sole candidate $F(v_{\parallel})$ is illustrated in the lower panel of Figure 14 had two humps, but the isocontour of the phase space in the top panel illustrates the complicated deformation of the distribution function that has produced such a double-peaked, reduced distribution in this higher angular three dimensionally resolved phase space portrait /24/. The actual $f(\mathbf{v})$ reflects coherent modifications at all pitch angles not just parallel acceleration. A similar situation occurs in the earth's foreshock /17/. While the time-dependent electric field plays a role in rounding the edges of the distribution function, the coherent deHoffmann-Teller frame electric and magnetic forces and their profiles produce the main inflation and distortion of $f(\mathbf{v})$.

Corollary of Electron Coherent Understanding at
Fast Mode Shocks: $\int B_y\, dx > 0$

Prior to the GS analysis the positive value of the integral involving the magnetic field in equation (7) had gone unnoticed. In the ten years since reference /1/ was published more than nine papers have examined the existence or size of the indicated integrals from the observed magnetic fields across fast shocks of every type, obliquity, and degree of criticality /26,39,40,11,41-45/.

There is by now no question that the 'B_y' integral in fast shocks is indeed positive as hypothesized by Goodrich and Scudder /1/ as a consequence of reasoning based on the different inertia of electrons and ions. It is also an observational fact for fast shocks that the NI potential jump exceeds that in the HT frame. The basic reason for electron heating being smaller than the flow energy lost by the ions decelerating across the shock is that $[\Phi^{\mathrm{HT}}]$ controls the inflation void formation of the ellipse of Figures 10 and 11 and it, in turn, for fast mode shocks is smaller than $[\Phi^{\mathrm{NI}}]$, that controls the ion energy loss.

THREE-DIMENSIONAL FLUX TUBES, FLOW LINES, AND COPLANARITY PLANES

Apparently part of the difficulty in accepting the GS suggestion for resolving the small electron energy gain was that $[R_{yB}] > 0$ involved the B_y, or "*out-of-coplanarity-plane*" component of the magnetic field. In some MHD expositions the so-called coplanarity plane is described as "containing" the low- and high-entropy flow field vectors and shock normal. MHD says nothing about the zero thickness shock layer except that magnetofluid variables need not be differentiable there, but must satisfy certain conservation or (Hugoniot) jump conditions. Considered as vectors, the inflow plasma velocity, $\mathbf{U_L}$, the magnetic field, $\mathbf{B_L}$, and the shock normal $\hat{\mathbf{n}}$ are coplanar. The high-entropy outflow vector, $\mathbf{U_H}$, the magnetic field, $\mathbf{B_H}$, and the shock normal are also coplanar. These two planes are both perpendicular to the conserved motional electric field tangential to the shock, $\mathbf{E_T}$. In the sense of vector fields, the *asymptotic* vectors $\mathbf{U_{L,H}}$, $\mathbf{B_{L,H}}$, $\hat{\mathbf{n}}$ meet the conditions for being coplanar; *this does* **not** *mean, however, that the plasma fluid streamlines and the magnetic field lines through the plane of the shock can be found in* **a** *common plane (cf. Figure 15a based on arguments in reference /33/.*

In spite of $B_y(x)$'s well-known presence in early two-fluid models of shock layers as cited by GS and summarized in 1971 /27/, various examinations of the logic of GS sought to find conceptual errors with the *existence, let alone the coherence of* B_y*, throughout the layer.* Cairns /26/ suggested that the GS analysis did not inexorably lead to the requirement on $\int B_y$, but could just as consistently be carried through assuming B_y vanished identically across the shock layer. Unfortunately, Cairn's algebra led to a downstream state with an asymptotic current /25/, an unacceptable description of a shock, the subject of the original GS analysis /1/. Despite finding the B_y signature predicted by the logic, electrodynamics and relativity arguments of GS /1/, despite acknowledging the published GS refutation /25/ of Cairn's specious argument that had nothing to do with shock layers which Thomsen repeated, Thomsen et al. /39/ sought to differentiate the "$\int B_y/B_x\, dx > 0$" GS reasoning /1,25/ from a theoretical argument of its requirement to occur in the shock layer. In addition to confirming the predicted effect in shock crossing magnetometer records and in simulations, they also noted that the handedness of the whistler precursor for a fast mode shock, with the shock ramp as the last half-wavelength, might explain the sign of the "B_y" integral. Curiously, these authors appear to have been unaware of the work summarized more than fifteen years earlier by

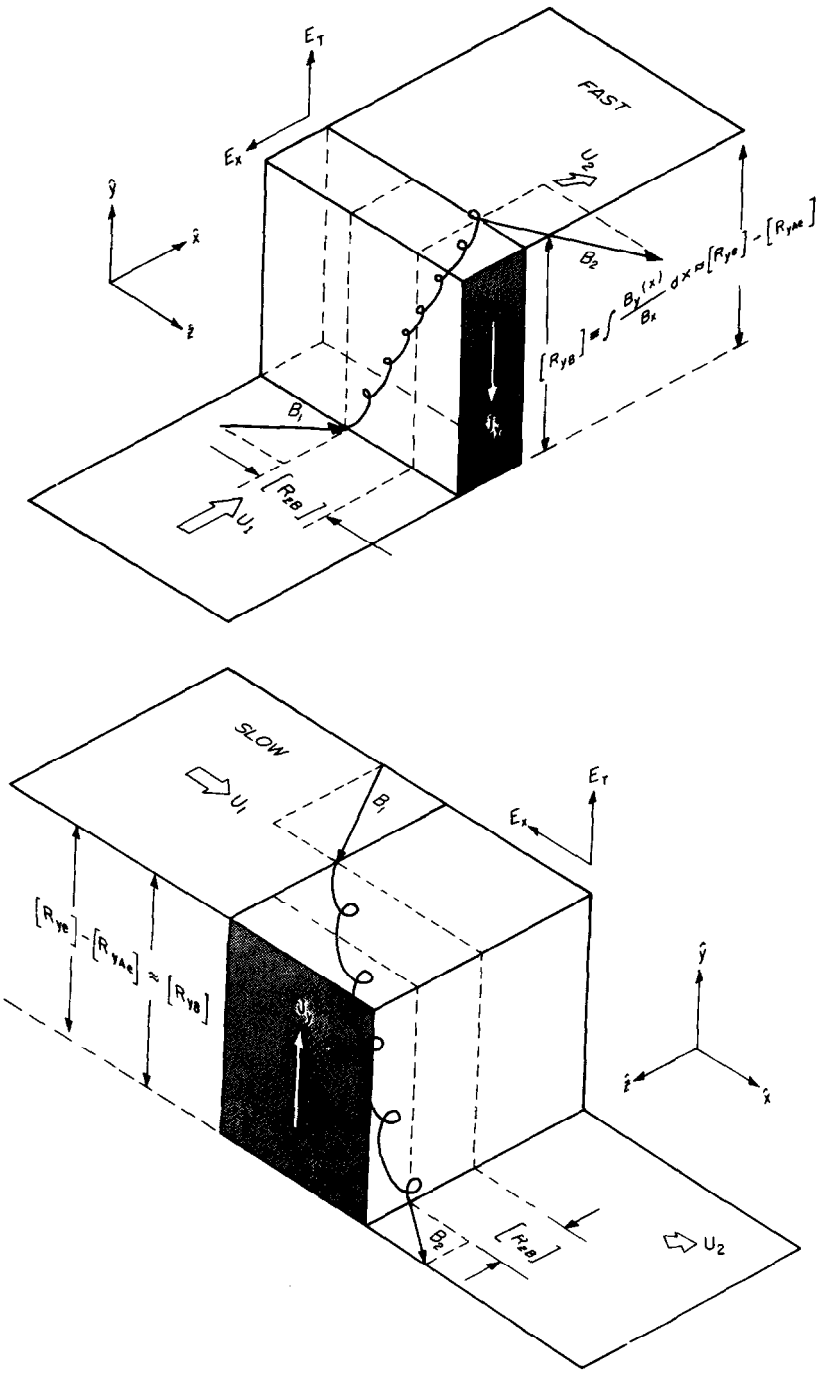

Fig. 15. Coplanarity "Steps" and $[R_{yB}]$ at (a) Fast and (b) Slow Shocks /33/.

Tidman and Krall /27/, cited by GS /1/, that showed layer magnetic hodograms of two-fluid shock solutions of the magnetic field as it rotates in an oblique shock from initial to final state. Two such solutions through the shock layer that clearly demonstrate the residual effect for $\int B_y$ as a result of the rotation are reproduced in Figure 16.

LAYER AVERAGED ION AND ELECTRON TORQUES

The nonvanishing displacement of the integral of (7) implies that the two aforementioned coplanarity planes are separated by a distance /33/

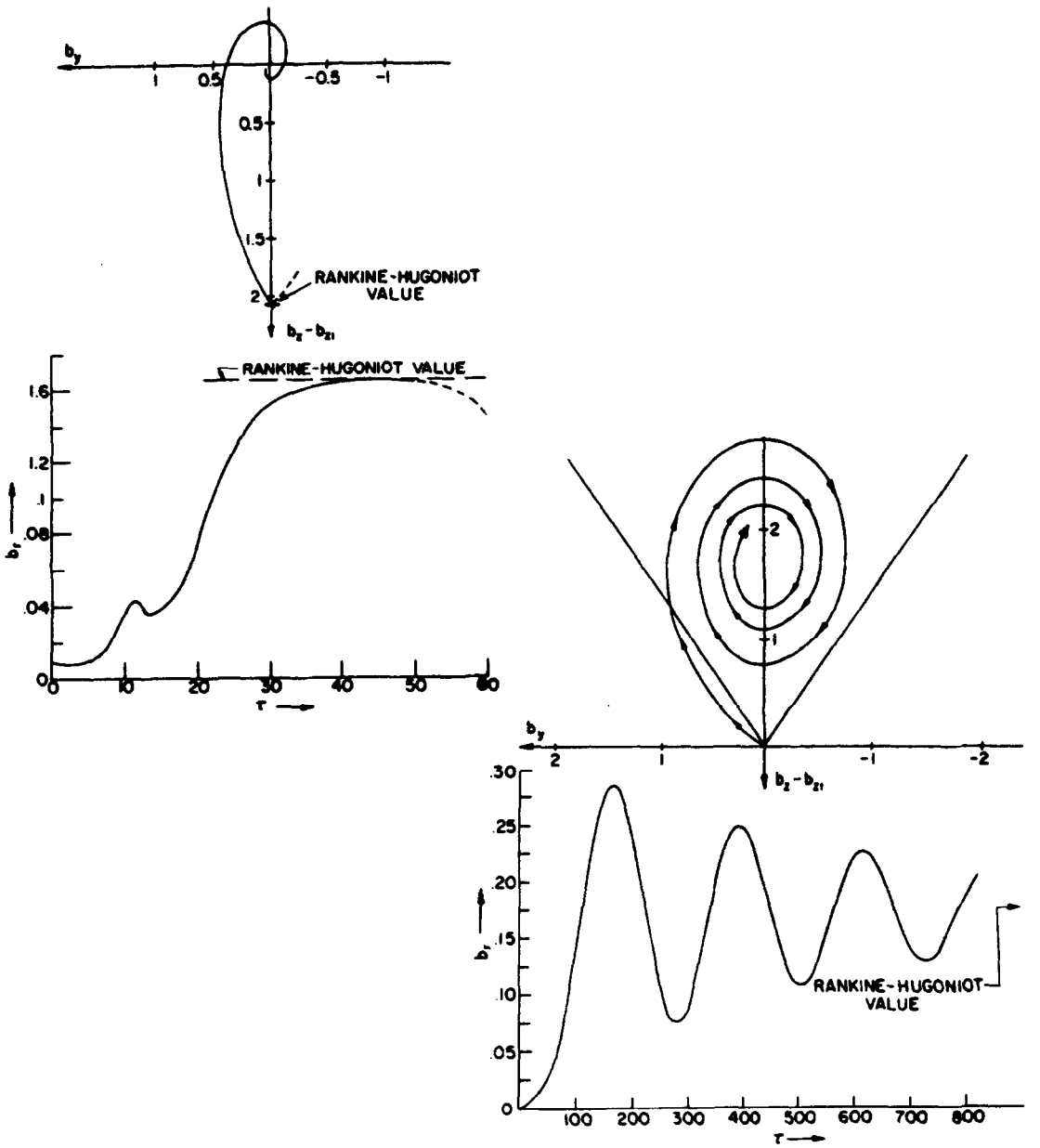

Fig. 16. Magnetic hodograms through shocks—two-fluid theory /27/. The hodograms of the transverse components illustrate the presence of *both* transverse components within the layer. Closer inspection illustrates that the $\int B_y dx$ also has a coherent value as well.

$$[R_{yB}] = \int \frac{B_y(x)}{B_x}\, dx\,, \tag{15}$$

that is, the net displacement of the magnetic tube of force along the tangential electric field direction as indicated in Figure 15a,b. Hence, the nonvanishing average of the *noncoplanarity* components of **B** within the layer reflects the departure of the magnetic tube of force from the "inflowing plane of coplanarity" enroute to the "exiting plane of coplanarity." The suggested components should be found within the layer that MHD treats as a discontinuity of zero thickness. In the case of the arguments of GS /1/ for fast mode shocks, the observations of **B** to determine this integral, or the direct determination of $[\Phi^{NI}] - [\Phi^{HT}]$ /23/, all agree that this displacement is positive, hence along $\mathbf{E}_T$.

Thought of as a geometrical entity the magnetic tubes of force within the layer have two "kinks" in two different projections: (i) that in the (x-z) plane, and (ii) that in the (x-y) plane. The kink, or refraction, in the (x-z) plane is the hallmark magnetic signature of whether the shock is a fast or a slow magnetosonic shock /46/; for the fast (slow) shock the magnetic field refracts away from (toward) the shock normal. As illustrated in Figure 15a,b, these different behaviors both correspond to positive $[R_{zB}]$ displacements of the tube of force along the $\hat{z}$ axis.

On the other hand, the kink in the (x-y) plane is the restatement of the sign and size of $[R_{yB}]$. The suggestion that $[R_{yB}]$ is positive at fast shocks implies that this kink in the shock layer has an average positive $\langle B_y \rangle$. For slow shocks the sign or size of $[R_{yB}]$ is still to be determined. The mean pitch and sense of these two projected kinks determine the initial torque in the $\hat{\mathbf{z}}$ direction, $\mathbf{V}_i \times \mathbf{B}$, on the ions that are basically hurdling in the NI frame across the shock along the normal.

The displacement of the flow lines of electrons and ions in this geometry of flux tubes is crucial to understanding the net energy available for the electron and ion heating. Scudder showed /33/ by explicit calculations that the electron flow line within the shock layer in the (HT) frame electric field is *almost precisely parallel to the magnetic field direction* provided three criteria are met, involving the electron's sonic number, the anisotropy of the shock, and the amount of the resistivity. Using data from a supercritical high-β shock the degree of misalignment through the layer was indeed small, only a few degrees at the worst location /33/. When the required assumptions are met, this extension of the HT theorem for electrons demonstrates that the NI electron flow line displacement (in the unaffected coordinates transverse to the HT frame transformation velocity) essentially track that of the field. This displacement for electrons in this $\hat{\mathbf{y}}$ direction is given by the expression

$$[R_{ye}] = \int_{t_1}^{t_2} \frac{V_{ye}(x)}{V_x(x)}\, dt \,. \tag{16}$$

When the extension for electrons of the HT theorem applies within the shock layer proper, the electron and magnetic flux tube displacements are virtually synonymous, viz.

$$[R_{ye}] \simeq [R_{yB}] \,. \tag{17}$$

In a fast mode shock this has the practical implication that in the NI frame, the electron gas must do work making progress along $\mathbf{E}_T$, giving up a significant amount of the energy it gained making progress across the ramp. From the larger perspective, the electrons that remain magnetized "hug" the tube of force as it appears to climb to the exit coplanarity plane. This understanding is similar to the statement that the electrons "largely" drift through the shock on equipotentials. In fact, the HT potential difference is precisely the residual number of equipotentials traversed because the electrons did not quite keep up with the meandering of the magnetic field. As in the usual understanding of frozen flux violations /47/, the existence of the ambipolar potentials cause this slight slippage between electron flow lines and the magnetic tubes of force. Figure 5 from GS depicts the topology of the electrical equipotential structures in the NI and HT frames. The staircase curves of Figure 5a represent a potential structure consistent with the total NI electric field; the vertical line equipotentials of Figures 5a (5b) are those of the NI electric field along the normal (HT total electric field). The motion of the electron flow line (in either frame) for a fast mode shock in this plane are nearly the same as the isocontours of the NI potentials, which is nearly synonymous [by (17)] with the projection of the magnetic tube of force in this plane.

Sense of Ion Torque and Sign of $\int B_y dx$

One physical meaning of $[R_{yB}] > 0$ has been developed above and in /33/ concerning the locus of the magnetic tubes of force that pierce the shock. A second related issue concerns the defining attributes of fast and slow shocks: the magnetic field is refracted away from (toward) the normal axis in a fast (slow) mode shock /46/. In the HT frame the flow is asymptotically parallel to $\mathbf{B}$. In this frame the outflow velocity is refracted away from (toward) the shock normal in fast (slow) shocks. Since the change in flow velocity is a Galilean frame invariant, we may write

$$[V_z] = [V_{ze}] = [V_{zi}] \geq 0 \quad \text{All Frames: Fast Shocks ; 0 for Perpendicular} \tag{18}$$

$$[V_z] = [V_{ze}] = [V_{zi}] < 0 \quad \text{All Frames: Slow Shocks .} \tag{19}$$

In the NI frame (with the inflow along the normal), the high-entropy flow vector must be deflected to the right (left) of its initial direction on transiting a fast (slow) shock. Thus $V_{z2}^{\rm NI} \geq 0$ (< 0) for fast (slow) shocks. The fluid ion acceleration along the z direction is in general given by

$$\int a_z dt = \int \left(\frac{e}{M} \frac{V_{ix}(x)B_y(x) - B_x V_{iy}(x)}{c} - \frac{\frac{d}{dx} P_{ixz}}{Mn(x)} \right) dt \,, \tag{20}$$

which can be rewritten using conservation of mass and $dt = dx/V_x$ as

$$[V_{zi}] = \Omega_{ci1} \cos\Theta_{Bn1} \left([R_{yB}] - [R_{yi}] \right) - \frac{[P_{ixz}]}{MnV_x} \,. \tag{21}$$

A similar expression can be obtained for the electrons, viz.

$$[V_{ze}] = \Omega_{ce1} \cos\Theta_{Bn1} \left(- [R_{yB}] + [R_{ye}] \right) - \frac{[P_{exz}]}{mnV_x} \,. \tag{22}$$

GS /1,25/ explicitly use [in their equation (5)] $[V_{iz}] = [V_{ez}]$, enforcing zero asymptotic current and had already used $V_{xi} = V_{xe}$ along the way in the condition on $[R_{yB}]$. Another corollary to zero asymptotic current is that the out of coplanarity plane integral that reduces the electron heating can be *completely* determined by the expression:

$$[R_{yB}] = \frac{M}{M+m} \left\{ [R_{ye}] - \left[\frac{c \sin\Theta_{Bn} \left(P_{e\parallel} - P_{e\perp} \right)}{enV_x B} \right] \right\}$$
$$+ \frac{m}{M+m} \left\{ [R_{yi}] + \left[\frac{c \sin\Theta_{Bn} \left(P_{i\parallel} - P_{i\perp} \right)}{enV_x B} \right] \right\} \,, \tag{23a}$$

where square brackets, as usual, denote jumps between asymptotic states. Gyrotropic, but anisotropic, asymptotic ions and electrons have been allowed in (23a). This expression should be contrasted with equation (6) of JE /40/ that claimed to be based on "first principles" even though it omitted the pressure anisotropy contributions of equation (23) and had the form in the present notation

$$[R_{yB}] = \frac{M}{M+m} [R_{ye}] + \frac{m}{M+m} [R_{yi}] \quad \text{[JE eq. (6)]} \,. \tag{23b}$$

Even the terms retained by JE above are **not** *separately, nor together theoretically determined by the Hugoniot jump conditions as they claim.* The published, rather than idealized attributes of collisionless shocks had disclosed that the anisotropy terms were also important in the downstream shock layer since the initial ISEE observations and the hybrid simulations /21/.

Adopting symbols $[R_{yAe}]$ and $[R_{yAi}]$ for the electron and ion anisotropy terms, (23a) can be succinctly summarized *without approximations* to be

$$[R_{yB}] = \frac{M}{M+m} \left([R_{ye}] - [R_{yAe}] \right)$$
$$+ \frac{m}{M+m} \left([R_{yi}] + [R_{yAi}] \right) \,, \quad [V_{ze}] = [V_{zi}] \,. \tag{24}$$

The remaining constraint on the current at the shock layer is the integral over Ampere's law, viz.:

$$\left([R_{ye}] - [R_{yi}] \right) = \frac{c}{M_A \omega_{pi}} \frac{[B_z]}{B_1} \quad \text{Ampere} \tag{25a}$$

$$= \frac{c}{4\pi |e| V_x} [B_z] \,. \tag{25b}$$

The latter form (25b) illustrates that as the Mach number increases, the *net* electron and ion y displacements get closer together. Either form demonstrates that this separation is positive

(negative) for fast (slow) mode shocks. It also suggests that this y separation for electrons and ions for strong shocks scales like the ion inertial length and inversely with the Alfvén Mach number of the flow. For slow shocks the maximum separation occurs at the switch-off limit.

Equations (25a,b) reflect what *can be known* from the one-fluid Hugoniot jump conditions. Equation (23) shows that the heart of the partition of energy between electrons and ions, $[R_{yB}]$, depends on information **not** available from the Hugoniot relations of one fluid nor from (25), contrary to published claims /40/.

Solving (25a) for $[R_{yi}]$ and substituting it into (24) yields

$$[R_{yB}] = [R_{ye}] - \frac{M}{M+m}[R_{yAe}] + \frac{m}{M+m}[R_{yAi}] - \frac{m}{(M+m)}\frac{c}{M_A\omega_{pi}}\frac{[B_z]}{B_1}\,. \tag{26}$$

For a proton plasma the leading order in m/M of (26) becomes

$$[R_{yB}] \simeq [R_{ye}] - [R_{yAe}]\,. \tag{27}$$

Equation (27) is an integral restatement of the layer interior corollary to the HT theorem /33/: the electron fluid element closely follows the magnetic tube of force inside the shock as well as in the asymptotic region provided the anisotropy is small. This has also been verified in /41/, where simulation results in fast shocks have been used to show (cf. Figure 17) the strong correlation of $\int B_y\,\alpha[R_{yB}]$ and the electron number flux $\int J_{ye} = -\beta[R_{ye}]$ through a shock layer. Empirically it has been shown /33/ that (27) is a close approximation to reality.

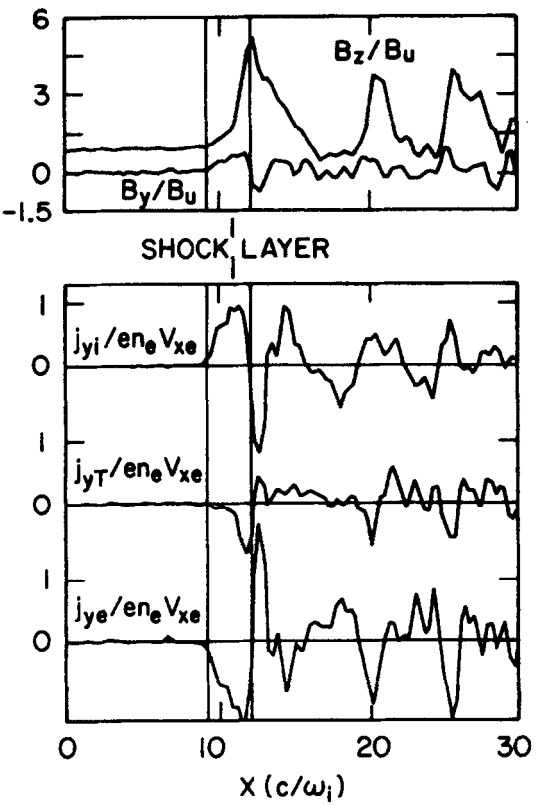

Fig. 17. Simulation demonstration that compares J_{ye} and $-\beta[R_{yB}]$ /41/.

Using (26) back in the ion and electron z deflection expression of (21) and (22) yields

$$[V_{zi}] = \frac{c\Omega_{ci}\cos\Theta_{Bn1}}{M_A\omega_{pi}}\frac{[B_z]}{B_1} - \frac{[P_{exz}]}{MnV_x} - \frac{[P_{ixz}]}{(M+m)nV_x}\,, \tag{28}$$

and

$$[V_{ze}] = \frac{c\Omega_{ci}\cos\Theta_{Bn1}}{M_A\omega_{pi}}\frac{[B_z]}{B_1} - \frac{2[P_{exz}]}{MnV_x} - \frac{m}{M}\frac{[P_{ixz}]}{MnV_x} . \tag{29}$$

Further consistency of equations (22a,b) requires to order m/M that

$$[P_{ixz}] \simeq [P_{exz}] . \tag{30}$$

By virtue of (30), the ion pressure anisotropy condition in (29) contributes negligibly to the electron fluid deflection when compared with the role of the electron anisotropy. *We thus obtain the view from* (21,30) *that the ions are torqued in the (x-y) plane by the disparate progress of the magnetic tubes of force and the ion flow lines in the y direction.* By (27) the field lines are carried by the electrons, so either the average $\langle B_y\rangle$ supplies the appropriate torque on the ion center of mass or the different rates of electron and ion progress represent a current in the $\hat{y}$ direction that exerts a J_yB_x torque on the center of mass, i.e., causes the ions to turn. In this view $\int B_y = \Delta x\langle B_y\rangle$ is a restatement in terms of the geometry of the tubes of force that one usually refers to as a "$\mathbf{j}\times\mathbf{B}$" force at the one-fluid level.

Because the ion V_z must be increased at a fast shock, and because the ion center of mass is initially momentum dominated, $[R_{yB}]$ being positive (determined by the mobility of the electron) can start to cause a $\mathbf{V_{ion}}\times\mathbf{B}$ force that deflects the ion flow line appropriately. Similar reasoning at a slow shock would suggest that the $[R_{yB}]$ being less than zero starts to torque the flow by reducing V_z. As a note of caution, however, the integral statements in (21) and (22) do not rule out that these displacements could be either up or down, since in the case of (20), all we are really sure of is that

$$[R_{yB}] - [R_{yi}] \geq (<)\ 0\ , \quad \text{Fast (Slow) Shocks} . \tag{31}$$

Equation (30) in (22) suggests that the change in the electron pressure anisotropy across the layer from the $[P_{exz}]$ term may be the principal determinant of the deflection of the electron fluid element. Even a very small downstream electron anisotropy, A_{eH}, in the subsonic electrons can produce an MHD scale deflection in the electron fluid element, viz.:

$$[V_{ze}] \simeq A_{eH}\frac{w_{eH}^2}{V_{xH}} = A_{eH}\frac{w_{eH}}{M_{eH}} , \tag{32}$$

where M_{eH} is the electron's exhaust Mach number, that is invariably *less* than unity. In this respect the precise high-entropy electron anisotropy may be viewed as the "fine tuning" of the tangential stress balance to ensure no asymptotic current flows. This, in turn, is closely related to the size of $[\Phi^{HT}]$ via (9).

Jones and Ellison (JE) tried to complete their claim /40/ that $\int B_y$ could be determined by Hugoniot parameters by reinserting Ampere's law (25a) into (27) (which for them never had anisotropy anyway) and then *neglect the terms that could not be known from Hugoniot* viz.:

$$[R_{yB}] \simeq [R_{ye}] \tag{33a}$$

$$= \frac{c}{4\pi n|e|V_x}[B_z] + [R_{yi}] \tag{33b}$$

$$\simeq \frac{c}{4\pi n|e|V_x}[B_z] \quad \text{(JE)} , \tag{33c}$$

discarding the $[R_{yi}]$ term of (33b) that is the $\int J_{yi}$ of the ion contribution to the current in the y direction—a term that **cannot** be determined from Hugoniot relations! The displacement of the ion center of mass caused by the downstream gyrating ions had been well known since the earlier simulation results /21/ and the initial ISEE observations five and ten years earlier, respectively. This neglected term is the same one that yields the difference between the Φ^{NI} and Φ'^{NI} curves in Figure 4. It had been suspected that this or some similar form of "viscosity" played a role in supercritical shocks from nearly the outset of collisionless shock work. The gyroradii of ions

larger than electrons and, as Ampere's form (25a) clearly demonstrates, the electrons and ions contribute on an *equal* footing to the integrated current. There is no a priori reason to neglect the ion's role in the layer currents as has been done by JE.

Perhaps even more curious is the endorsement of JE's explanation by Gosling and coauthors /41/, after they demonstrate the order of magnitude error made by JE (going from equation (33b)–(33c) to achieve a "result" dependent only on Hugoniot. The comparison done with observed shocks /41/ is reproduced in Figure 18, where the logarithm of observed values (from almost exclusively supercritical shocks) of $[R_{yB}]$ were typically 10 times that predicted by the JE equation (31c). The lowermost diagonal line would be confirmation of the JE first principles derivation. Either the data are suspect, or the derivation is not a first principle one. Subsequent analysis of *subcritical* shocks /42/ shows a more favorable agreement with the *approximate* JE expression in terms of Hugoniot. Clearly, if you knew that resistive shocks did not need reflecting gyrating ions, you would have some leverage to suggest the approximation made by JE. It is surely not a general first principles understanding as Gosling et al. clearly illustrate, their endorsement notwithstanding. To this point Jones and Ellison /43/ finally concede four years later that their result was incomplete.

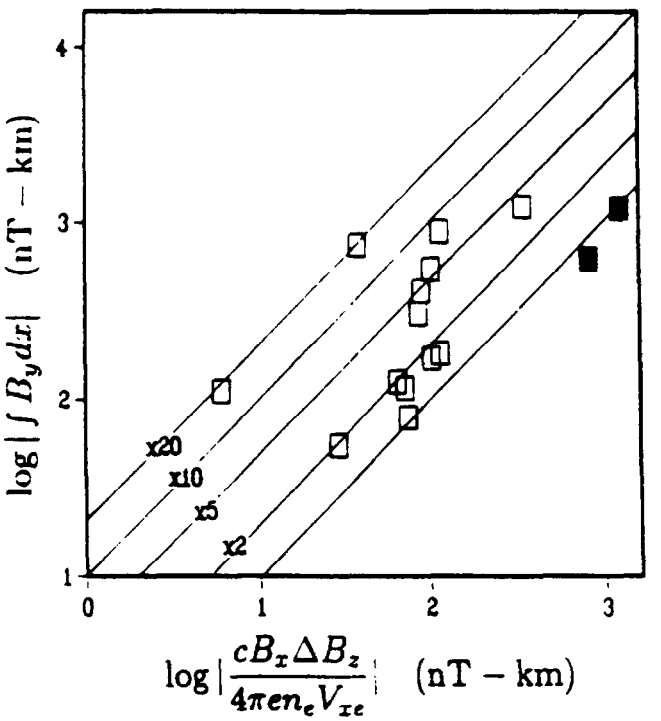

Fig. 18. Comparison /41/ of $\log B_x[R_{yB}]dx$ versus its size predicted by Jones and Ellison /40/. Solid squares are marginally critical shocks. *All* supercritical shocks miss the "first principles" theoretical formula of Jones and Ellison by factors of 2–20.

Goodrich and Scudder /1/ exploited the disparate electron and ion masses to suggest that the magnetized electrons can gain considerably less energy from the fast mode electric field than the unmagnetized supersonic ion beam loses in directed energy. As a corollary to this understanding and the observed different energy gain to electrons and lost by the transmitted solar wind beam, they correctly predicted the coherence and sign of $\int B_y$ for the noncoplanarity component of **B** across fast mode layers. The "first principles" derivation of JE, endorsed by Gosling et al. /41/ and Freidman et al. /42/, repeatedly assumes (1) small mass ratio arguments and neglects pressure anisotropy growth to obtain (33a) without any a priori regard for, or knowledge of, the ion flow lines displacement $[R_{yi}]$ in the $\hat{y}$ direction, and (2) then for the convenience of proving the assertion of a first principle derivation for $[R_{yB}]$ dependent only on Hugoniot, drops a well-known and large term, $[R_{yi}]$. Curiously Gosling et al. /41/ conclude "... We find substantial support for their [JE]

suggestion that the field rotation [out of the plane] and thus also the frame dependence of the potential drop are fundamentally a consequence of unequal electron and ion masses."

Goodrich and Scudder /1/ correctly identified the inertial mismatch of the electrons and ions as the key to their suggestion of the relevance of the two different frames, and $\int B_y > 0$, for the electron heating at fast mode shocks. On all accounts, without foreknowledge of the outcome, GS's theoretical reasoning and observations led to a well-framed hypothesis that has been independently and amply verified. In this review an attempt has been made to give the $\int B_y$ effect a geometrical reality in terms of the displacement of the tube of force between entrance and exit planes of coplanarity and to illustrate its indispensable role in actually implementing the required tangential acceleration to the ions.

Slow Shocks

Many of these same ideas developed for fast shocks can be used for understanding slow shocks. While slow mode shocks in the solar wind are rare at and beyond the orbit of the earth, they have more frequently been identified in the magnetospheric context in the ISEE data /48-51/. The electron observations, now routine, were made across these structures. When the *ion* measurements are available, the electrons once again are clearly heated, but less so than the ions. In contrast with the fast shock morphology, the electrons are heated by an amount more than the estimated energy liberated by the deceleration of the bulk flow along the normal! The electron $f(\mathbf{v})$'s across the structures studied /48-50/ have beam-like features as do the fast mode shocks (cf. Figure 19). These beams were used /11/ to estimate the $[\Delta\Phi^{HT}]$ at slow shocks and these estimates were satisfactorily compared with that from the polytrope method. The inferred sign of the associated HT electric force on the ions is in the same direction as that in the NI frame. If the NI normal electric field, E_x, is limited, as in fast mode shocks, to be a fraction of the incoming ion bulk energy along the normal, then there is evidence that

$$[\Delta\Phi^{HT}] > [\Delta\Phi^{NI}] \quad \text{(Slow Mode Electron Observations)} . \tag{34}$$

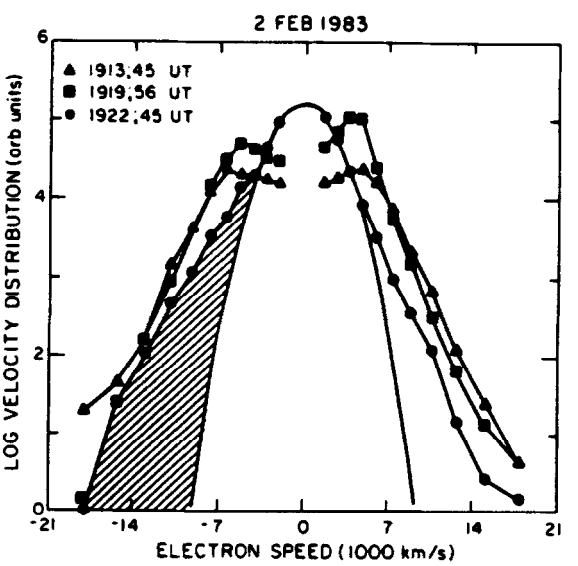

Fig. 19. Slow mode beams on electron distribution functions /48/.

This implies from equations (6) and (7) that $[R_{yB}]$ must be negative for slow shocks, and that the net electron energization comes by their net displacement opposite to the direction of $\mathbf{E}_T$. In support of this inference, a slow shock at the magnetopause discussed by Walthour et al. /51/ has been analyzed for this review (Figure 20 courtesy of C. T. Russell) to illustrate that indeed the $[R_{yB}]$ signature is opposite to that for fast mode shocks that has already been amply verified

consistent with this picture. (In the n, m, l coordinates, the expression for $[R_{yB}]$ takes on the form

$$[R_{yB}] = -\int_{\text{Low Entropy}}^{\text{High Entropy}} \frac{B_m}{B_n}\, dx\ , \tag{35}$$

where the minus sign arises from the definition of this coordinate system that places n and hence increasing x along the outward normal from the magnetopause or shock, directly opposite to the x direction of the NI coordinate system defined by GS /1/.) Such a signature would support the sense of the step discontinuity between the coplanarity planes indicated in Figure 15b above.

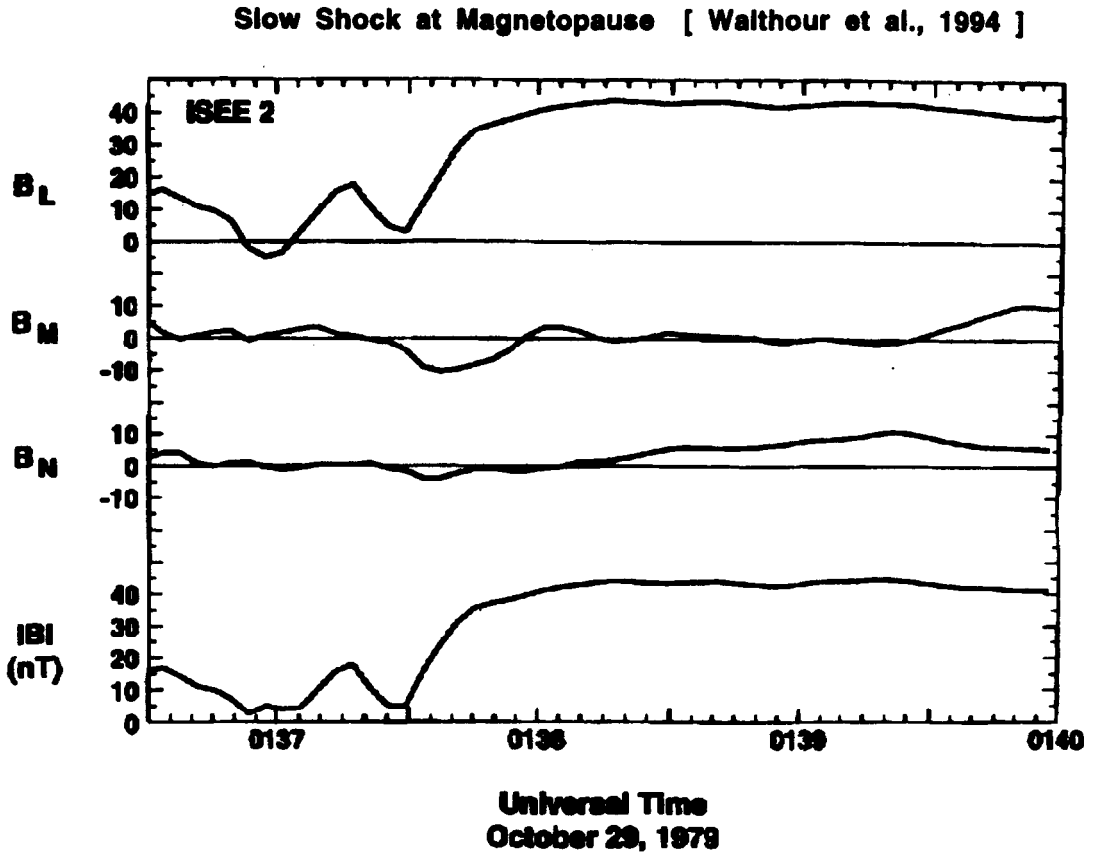

Fig. 20. Boundary normal plot of shock layer suggested /51/ to be a slow mode shock at the earth's forward magnetopause. This example as discussed in the text is an example of $[R_{yB}] < 0$ at a slow shock. Plot courtesy of C. T. Russell.

When witnessed in the interplanetary medium, slow shocks are traditionally thicker than fast mode shocks /52/. This suggests that the electrons would be even more strongly magnetized in these structures than in the thinner, well-documented fast mode shocks discussed above. Presupposing $m/M[R_{yi}] \ll [R_{ye}]$ and retaining pressure anisotropies would suggest for the slow shock that

$$[R_{yB}] \simeq [R_{ye}] - [R_{yAe}] \quad \text{(Slow)} \tag{36}$$

and Ampere's law requires that

$$[R_{yi}] > [R_{ye}]\ , \tag{37}$$

so that the magnetic field refracts toward the normal. Strong ion heating suggests that $[R_{yi}] > 0$ may be necessary at slow shocks to provide the observed heating.

A useful simplification of $[R_{yAe}]$ in (36) above can be made, if isotropy (gyrotropy) upstream (downstream) is assumed. In this situation this expression can be written in terms of the shocked

electron pressure anisotropy, $A_{eH} \equiv P_{eH\parallel}/P_{eH\perp}$ in the form

$$[R_{yAe}] = \sin\Theta_{BnH} \frac{A_{eH} - 1}{M_{eH}} r_{eH} , \tag{38}$$

where $M_{eH} \equiv V_{xH}/w_{eH\perp}$ is the shocked electron sonic Mach number, and r_{eH} is the shocked gas electron thermal gyroradius for a particle of the perpendicular thermal speed. All three factors in slow shocks *increase* across the layer and are positive. Particularly near the switch-off limit, this term could predominate over the electron $[R_{ye}]$ displacement. Being positive, it contributes a negative displacement in (36) for $[R_{yB}]$ in slow mode shocks. Enormous pressure anisotropies have been documented /51/ at slow mode shocks, testifying to the possible importance of this term.

In the HT frame the ion inertial effects control the persistence of the ion flux, so that currents must initially come from the electrons. The $\mathbf{E}_x^{\rm NI} \times \mathbf{B}$ drift is much weaker in the slow mode case than in the fast shock case. Furthermore, it is in the wrong direction for this to be the dominant guiding center drift of electrons as the complete support of the slow mode cross field current. *In the presence of anisotropy*, curvature drifts are another possibility that accomplish two things simultaneously: they cause the electron fluid to drift in the $-\hat{y}$ direction and successfully overcome the electric and betatron drifts to (1) supply a positive contribution to the j_y current necessary for the shock, and (2) at the same time gain adequate energy from $\mathbf{E}_T$ to be consistent with enough enhanced electron pressure to make $[\Phi^{\rm HT}] > [\Phi^{\rm NI}]$, as has been reported /11/. The inferred sense of the electric field and the decreasing magnetic field also imply, according to Liouville mapping consideration that led to the elliptical void for fast shocks, that the transmitted electrons will be more forward focused (cf. Figure 21) and more anisotropic than the fast mode shocks, favoring $T_\parallel - T_\perp > 0$ on shock transit. Notice that [ ] implies an integral across a layer which if thicker can give rise to large potential jumps even if $E_{\rm slow}^{\rm HT}$ were comparable to that in the NI frame.

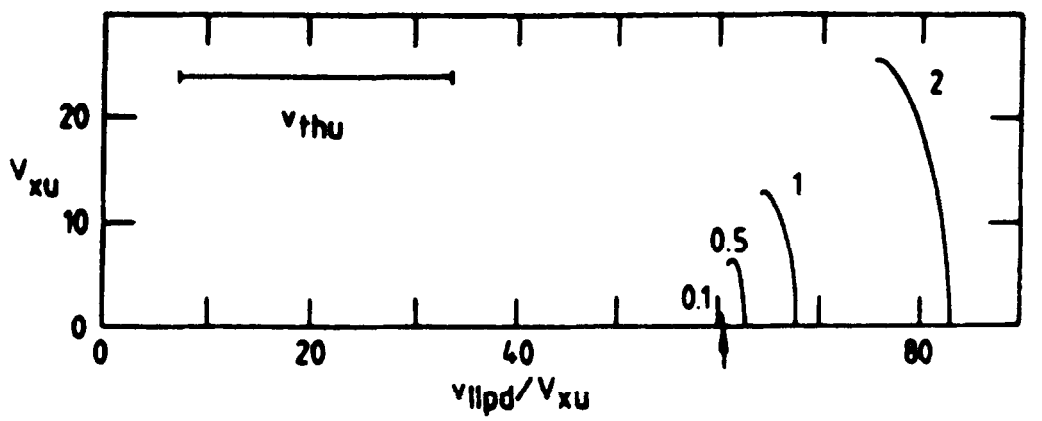

Fig. 21. Schwarz /11/ slow mode phase space mapping.

Because the electrons are expected to be more magnetized than in fast shocks, the observations require that $[R_{yB}] \simeq [R_{ye}] - [R_{yAe}] < 0$, but $|[R_{ye}]|$ could be larger or smaller than the $[R_{ye}]$, particularly if the ion flow line is displaced along $+\hat{y}$, which seems likely since any excess ion heating beyond that available from deceleration (which is small for slow mode inflows) must come from the positive ion displacement of R_{yi} along $\mathbf{E}_T\hat{y}$.

This translates into the inference that

$$[\Phi^{\rm NI}] - [\Phi^{\rm HT}] \simeq |\mathbf{E}_T|([R_{ye}] - [R_{yAe}]) . \tag{39}$$

The second term on the right-hand side is the average y displacement of the guiding centers in the y direction associated with the Finite Larmor Radius (FLR) corrections for curvature and gradient B drifts within the shock layer. In the presence of strong anisotropy $[R_{yAe}]$ may be more important

in determining the field displacement than the net displacement of the electron center of mass. Solving for the HT potential jump

$$[\Phi^{\mathrm{HT}}] \simeq [\Phi^{\mathrm{NI}}] - |\mathbf{E}_T|([R_{ye}] - [R_{yAe}]) , \tag{40}$$

together with observations in fast shocks of [Φ's] that

$$[R_{ye}] - [R_{yAe}] > 0 \quad \text{Fast Shocks} , \tag{41}$$

while there are suggestions /11/, and Figure 20 also suggests a similar interpretation, we tentatively conclude that $[\Phi^{\mathrm{NI}}] \ll [\Phi^{\mathrm{HT}}]$ in slow shocks so that

$$[R_{ye}] - [R_{yAe}] < 0 \quad \text{Slow Shocks} . \tag{42}$$

Summarizing, it would appear possible that the sign of $\int B_y dx$ across the shock layer is the hallmark of the x-z plane turning action felt by the ions. Since that turning sense is required to be opposite for fast and slow shocks, the sign of this integral should reverse between the two classes to implement the different torques. Starting in along the normal, the fact that B_y has an average sense through the layer gives an average sense to the torque on the ion fluid in the (x-z) plane with an approximate magnitude given by

$$\frac{\Delta V_{z,i}}{\Delta t} \simeq \frac{B_x V_{xi}}{Mc} \frac{[R_{yB}]}{\Delta x} \hat{\mathbf{z}} . \tag{43}$$

If coherent B_y builds up before the ions are dissuaded from moving along the normal (43) gives the correct sense of the refraction of the ions at the shock wave. This argument will be more complete in the limit of negligible gyrating ions.

SIMULATIONS AND ELECTRONS

Hybrid simulation codes with fluid electrons have until recently yielded little specific insight into the issues of electron heating and no information about the downstream distribution function. Some simulations required so much resistivity with fluid electrons while recovering the magnetic profiles /53/ that they grossly contradicted the observed electron/ion heating morphology at these same class of shocks (cf. /54/). Until recently, various hybrid codes have reassigned the available code simulation directions to allow various instabilities to be self-consistently included (to the exclusion of modeling the entire shock layer) with no success in recovering the observed flat-topped distributions. Forslund and Shonk /55/ had recovered such distributions in one-dimensional electrostatic shocks using $M/m = 1836$. Dum et al. /56/ found that the flat-topped electron distributions of the form

$$f(v) = \exp\left[-\left(\frac{v}{w_0}\right)^s\right] , \quad s \simeq 3.6 - 4$$

were the asymptotic solutions to fully developed ion-acoustic and Coulomb collision mediated transport, but neither these effects nor the acoustic instability was found in the simulations. Feldman et al. /14/ fit the observed flat-topped distributions to such theoretical predictions, but there are several alternate ways to make such flat distributions. Such fits do not uniquely identify acoustic behavior as the relevant cause.

The limitations of the geometry of the initial implicit particle-particle $M/m = 100$ code /57/ and its adaptation in Winske et al. /58/ that excluded the shock layer formation were reviewed in light of the observations /24/. Aside from modest suprathermal tail enhancement from the modified two-stream instabilities of the reflected ions, little experimental support was found in the observations for the effects that these simulations described. Winske et al. did retrieve a flat-topped electron distribution function, but they were not studying a self-consistent shock layer. Particularly disturbing was the absence on the shocked side of the magnetized particle solutions of the signature of the flat-top electron phase space in the Forslund et al. /57/ simulations with finite mass.

Recently Savoini and Lembege /45/ reported an explicit particle-particle plasma simulation for 1D and 2D oblique shocks with $M/m = 42$. This is the first reported magnetized simulation

that recovers the flat-topped electron distribution functions, while solving for the electromagnetic shock structure at the same time. They concur that the B_y coherence of GS is present and they concur with experimental work that can comment on their work /14,19,23,24/ that the coherent forces at the shock overwhelmingly determine the electron heating across the shock. This argument is made by rotating the simulation axes so as to preclude the resistive collective effects and demonstrating that the flat-topped distributions are still recovered. At $\Theta_{BnL} = 55°$ they find the ratio of $[\Phi^{HT}]/[\Phi^{NI}] \simeq 0.4$ The precise reason for the recovery of flat-topped distributions in these simulations versus the implicit code of Forslund et al. /57/ was not completely elucidated.

Computer codes represent their own compromises. During the B_y controversy there was considerable faith placed in code results to demonstrate the size of the B_y, irrespective of its fidelity to produce other observables about electrons /39,41/. Since $\int B_y$ is intimately connected with both the net electron heating and the regulation of zero current, the simulations were stopping the current along the shock normal in some other way—a way different than occurs in nature! In this respect the most recent simulations of /45/ *that recover the observed flat-topped distributions while producing the shock* are the first simulations to have adequate internal consistency to estimate the $\int B_y$ in a way that can evaluate the GS explanation. They have strongly endorsed from their diagnostics the role of B_y and the coherent DC cross shock potential for the formation of the signature flat-topped electron distribution function.

STATISTICAL WORK

Many authors /39,11,59,41/ have used the approximate formula (10) to *estimate* the HT potential jump in the ensuing years. This approach ignores the significant changes in the pressure anisotropy, resistivity, and inertial corrections within the shock layer (cf. /24/). These layer proper effects should be resolved and the actual integral of equation (9) evaluated for high-precision comparisons of $|e|[\Phi^{HT}]$ with features such as beams on the distribution function or determinations of the precise relative size of the NI and HT potentials (see below). This cross check has been performed /59/ with the polytrope approximate method for the HT potential of formula (10) with the beam's kinetic energy to baseline the approach. The beam method was 20–30% higher than the that determined by (10). As much as one-half of this error was attributable to the wide polar angle of the analyzer used and a portion of this discrepancy may be connected with the channel spacing and effective bandwidth of the energy steps used. These results represent further confirmation of the suggestions of Goodrich and Scudder /1/ and Scudder et al. /24/ and much better agreement than the initial comparisons in the Feldman and coauthors' /14/ survey that in retrospect incorrectly compared the beam energy with the $[\Phi^{NI}]$. This cross check improved precision further when performed with the slow shock transitions that have been reported in the magnetotail /11/, where the potentials are larger and the issues of energy width and spacing may not have been as important.

The statistics show no strong organization of $[\Phi^{HT}]$ except with $[T_e]$, which was the major conclusion of Goodrich and Scudder /1/. However, statistics clearly showed the organization of the electron temperature increase Figure 22a as correlated with the change in flow energy along the shock normal, or more cleanly as approximately 20% of the available nondirected energy, ΔT_{tot} (Figure 22b).

Another trend noted /59/ was that at low *electron* Mach numbers (Figure 22c) the high-entropy side electron temperature achieved a value *as if being magnetized meant* that the downstream temperature should be

$$T_0 = \frac{1}{3}\left(2\frac{B_H}{B_L}T_{L\perp} + T_{L\parallel}\right) . \tag{44}$$

Departures from this "recipe" (dotted line in Figure 22c) for increasing electron Mach number have been noted /59/ and primarily in the presence of low-upstream β_e. As discussed previously /24/ and reaffirmed by Schwarz et al. /59/, there is no a priori expectation that the magnetization of individual particles in the presence of $E_\parallel$ implies that T_0 is the unheated or "adiabatic" result for the electron fluid. In particular, such reasoning implies strong electron pressure anisotropies behind the strong shock ($A \simeq 1/4$) that are not observed. Such an argument undercuts the Louiville

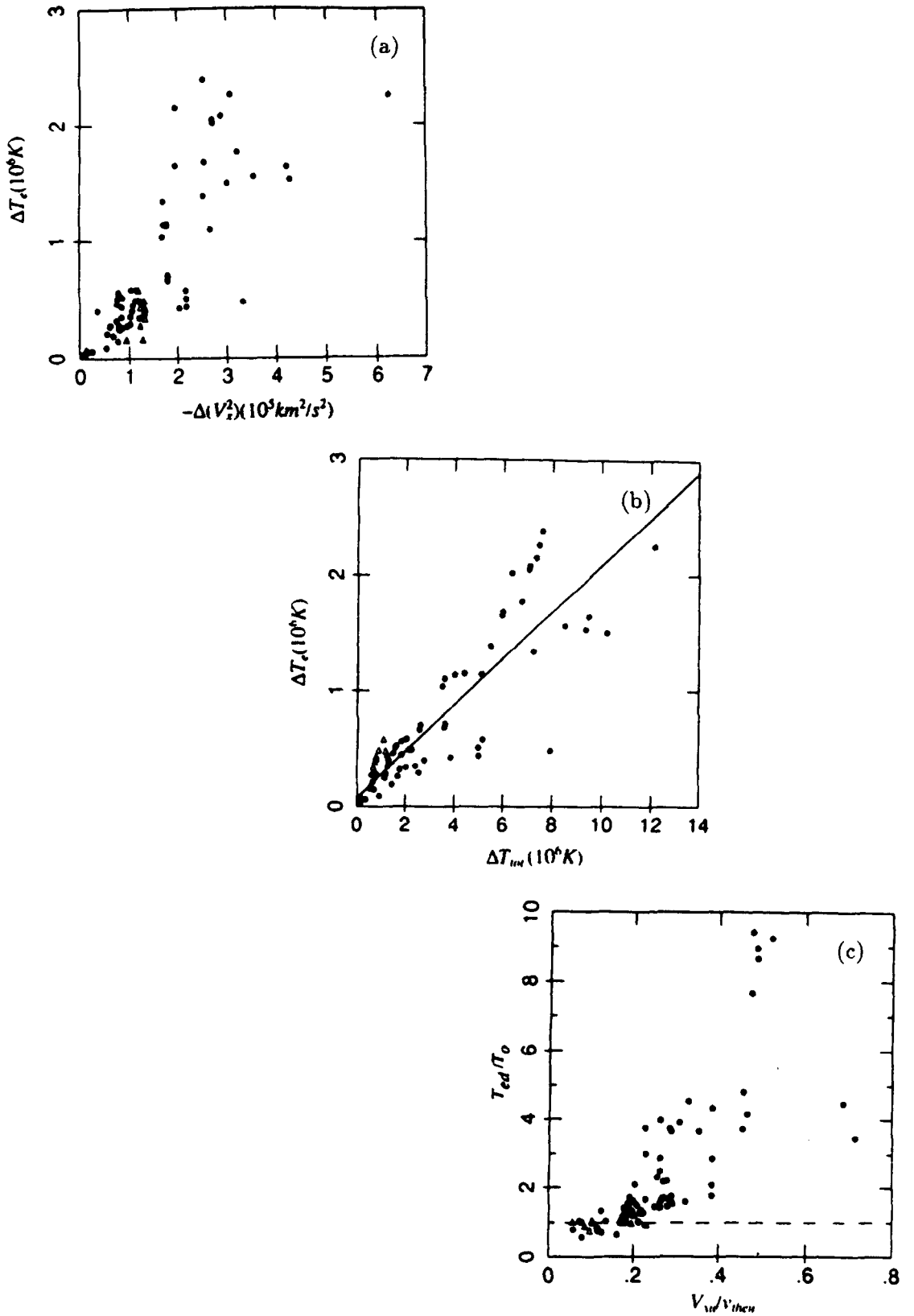

Fig. 22. a,b,c Statistical correlation of electron heating signatures /59/.

mapping ideas that are the underpinnings of the "beam" identification and the phase space mapping discussed above. In this respect T_0 has an ad hoc character that makes departures from it of unknown significance. It remains to be seen whether the departure of the data from the T_0 recipe (without theoretical foundation) implies deficiencies of the recipe, or our understanding of the coherent heating in the potential.

Relative Size of NI and HT Potentials—Statistics

Indirect attempts /39/ to get a statistical body of data for $[\Phi^{NI}]$ (without measuring the electron bulk motion) have been made. Their approach has been to approximate $[\Phi^{HT}]$ by equation (10) followed by

$$[R_{yB}] \simeq \int_{t_1}^{t_2} \frac{B_y(t)}{B_x} \frac{dt}{\mathbf{V}_{rel}\cdot\hat{\mathbf{n}}} \tag{45}$$

to estimate $[\Delta\Phi^{NI}]$ from equation (6). Many fast shocks have been catalogued in this rough manner.

All reported cases concur that the *sign* of $[R_{yB}]$ was positive as predicted by Goodrich and Scudder /1/. The resulting precision of $[\Phi^{NI}]/[\Phi^{HT}]$ must, however, be viewed with caution. Numerous untested assumptions have been made to determine $[\Phi^{NI}]$ in this way (polytrope γ_e, neglect of anisotropy, dissipation, the choice of interval $[t_1, t_2]$ for the $\int$, the shock normal accuracy, relative speed determination, and issues of stationarity).

ELECTRON BEHAVIOR AT HIGH MACH NUMBER SHOCKS

High Mach Number (HMN) Shocks are those where the electron inertial energies in the deceleration are important. This is a regime where the Alfvén Mach number, M_A, exceeds $(M/m)^{1/2}$. They have not been sampled with spacecraft but are thought to occur in supernovae explosions. In these shocks there will be energy jump differences between HT and NI frames. The corollary to the HT theorem discussed by Scudder /33/ will be vacated and the electron flow line will increasingly depart from being guided by the magnetic tube of force, availing more of the NI electrical potential for energization of the electrons. Fully relativistic and electromagnetic low-beta, particle-particle simulations of this type were reported by Tokar et al. /60/; the flow speeds reflected electron sonic Mach numbers of $M_A \simeq 60$. In this limit the electrons have some of the complicated behavior of the ions, having $\mathbf{E} \times \mathbf{B}$ drift speed gyroradii comparable to the scales of weaker supercritical shocks. Stronger absolute heating as a result of more serious violations of frozen flux were observed, but a reduced fraction of the available pressure increase was found to migrate into the electrons.

Schwarz et al. /59/ have sought, as in Figure 22c, to show that T_{ed}/T_0 is organized by the electron sonic Mach number, M_e. This *may* be viewed by some as part of a progression toward the HMN results presented by Tokar. In fairness, however, the simulations reported by Tokar were for conditions of $M_A \simeq 60 > (M/m)^{1/2}$ and are not comparable to the shocks considered in the Schwarz et al. study where $M_A < 10$.

POSSIBLE NONADIABATIC EFFECTS FOR SUPERCRITICAL BOW SHOCKS

Belikhan and Gedal in (BG) /61,34/ sought to identify coherent, but nonadiabatic, effects as the cause of the electron heating and the flat-topped electron distribution function at the earth's bow shock, where M_A is considerably below the regime investigated by Tokar et al. These authors have studied classes of electron trajectories through ad hoc static models of the magnetic and electric fields within the shock layer. Their focus has been the attempt to identify the consequences of nonlinear dynamics that they call a *trajectory instability*, whereby there was a breakdown in guiding center approximation. This regime has been studied by Cole /62/ and the condition for its existence was that the gyroradius of a particle with the speed given by $V_D = c(E/B)$ be larger than the scale of the electric field in the layer.

In symbols this condition is

$$\frac{c\frac{E}{B}}{\Omega_{ce}}\frac{1}{E}\frac{dE}{dx} > 1 \tag{46a}$$

or

$$\frac{1}{B\Omega_{ce}}\frac{d}{dx}\left[\hat{x}\cdot(\mathbf{V_e}\times\mathbf{B})\right] \simeq \frac{V_e}{L_B\Omega_{ce}} \simeq \frac{175\,\mathrm{km/s}}{6597\,\mathrm{km/s}} = 0.026\,, \tag{46b}$$

using parameters of the shock discussed in the literature /23/.

An alternate view of this condition evaluated at the center of the magnetic ramp is

$$\frac{V_D}{L_E\Omega_{ce}} = \frac{c}{B\Omega_{ce}}\left|\frac{d^2\Phi^{\mathrm{NI}}}{dx^2}\right|_0 > 1 \tag{47}$$

or

$$\simeq \frac{\xi}{2}\frac{M_A^2}{\left(1+\frac{[B]}{2B_1}\right)^2}\left(\frac{c}{\omega_{pe}D}\right)^2\,, \tag{48a}$$

where

$$\xi = \frac{\Phi^{\mathrm{NI}}(x=D) - 2\Phi^{\mathrm{NI}}(x=0) + \Phi^{\mathrm{NI}}(x=-D)}{0.5MV_{x1}^2}\,, \tag{48b}$$

and D is the half-width of the *narrow magnetic ramp* at the shock.

Conditions (48a,b) illustrate the simultaneous role in the nonadiabatic condition of the *curvature*, scale, and size of the NI electric potential *across the magnetic ramp*. Direct determinations of the cross shock potential and theoretical determinations of this profile (cf. Figures 2, 4b, 7b) show that the change in Φ^{NI} across the magnetic ramp is *nearly linear* (that causes $\xi \to 0$) and in any case small. Ignoring the curvature *issue*, BG have estimated the term

$$\frac{d^2\Phi^N}{dx^2} \simeq \frac{\Phi^{\mathrm{NI}}(+\infty) - \Phi^{\mathrm{NI}}(-\infty)}{2\mathrm{D}^2} \equiv \frac{[\Phi^{\mathrm{NI}}]}{2\mathrm{D}^2} \quad (\mathrm{BG})\,, \tag{49a}$$

in a way that inconsistently places one-half the asymptotic NIF jump across the magnetic ramp scale! Notice that in the limit as $(D \to 0)$ that (49a) does not pass over to the second derivative as does ξ in (48b). The actual change in the NI potential across the magnetic ramp of thickness 2D is given by the much smaller number

$$\Phi^{\mathrm{NI}}(x=D) - \Phi^{\mathrm{NI}}(x=-D) = [\Phi^{\mathrm{NI}}]\frac{2\mathrm{D}}{\frac{V_{xL}}{\Omega_{CiH}}} \simeq \frac{1}{40}[\Phi^{\mathrm{NI}}]\,. \tag{49b}$$

The neglected assessment of the determination of the curvature in the potential reduces the number even farther.

Since the NIF potential depends on the reliability of $\mathbf{V_e}$, this same observational paper demonstrates that this electric drift velocity has been measured two different ways through the shock and shown to agree /23/. This drift speed is small compared to the ion sound speed, let alone the electron thermal speed. Finally, Figure 9 illustrates that the particles with thermal energies have gyroradii everywhere less than 10 times the scale of $|\mathbf{B}|$ at the highest time resolution through the shock. Because the electric drift speed is everywhere subelectron thermal speed, this implies that the nonadiabatic assumption of BG is not satisfied by an even larger margin!

Balihkin and coworkers have erroneously considered an ad hoc shock layer model with the structure of the magnetic and electric fields set more or less by convenience. In particular, these authors localize the entire NI potential jump across the much shorter magnetic ramp of width 2D, so that $\xi_{\mathrm{BG}} = CIIL_H/2\mathrm{D} \simeq 10$ times too large (neglecting the issue of curvature). Further, these authors have not shown that the assumed magnetic and electric structures are consistent with being a shock,

because they have not verified that the assumed ensemble of forces at the modeled oblique shock transmits the same number of ions as electrons across the layer. If this cannot be demonstrated, then the observed simulations do not reflect a time stationary ensemble of fields and thus do not pertain to a one-dimensional shock.

Figure 23 illustrates the observational situation /19/ at supercritical shocks that BG are attempting to synthesize. There are many scales within the shock layer, but the main magnetic ramp is the shortest scale in the system; this is the physical layer that has been used by BG to be a layer of width 2D. *The observed magnetic overshoot takes place on a much longer scale, that of the convected ion Larmor radius in the perturbed magnetic field*: $L_{CIIL,2} = V_{xL}/\Omega_{ciH}$. Since the early hybrid simulations /21/, it has been known as the scale of the overshoot and for the typical quasi-perpendicular bow shock at 1 AU has a length of $\sim$ 174 km. The scale of the undershoot in the magnetic intensity below the Hugoniot value, takes place on the much larger convected inertial

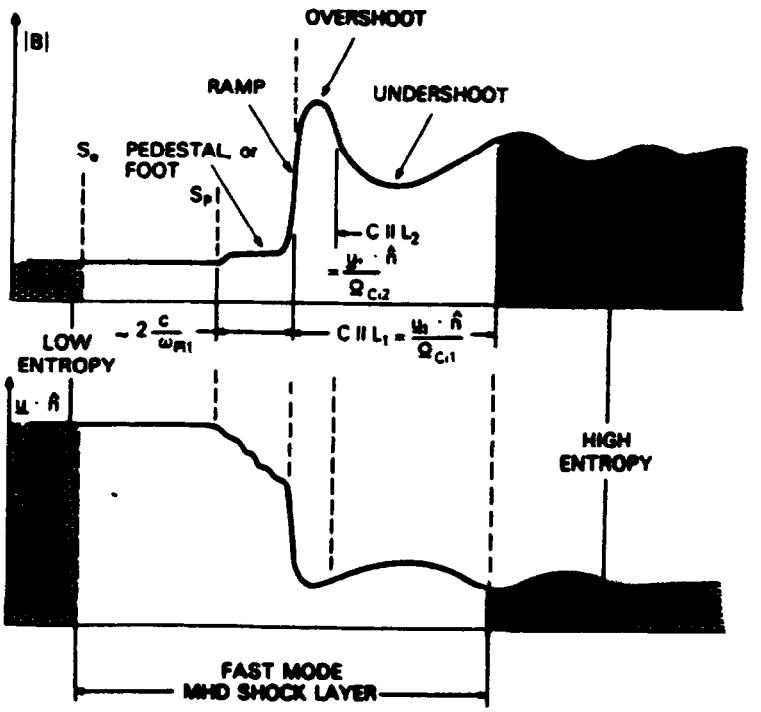

Fig. 23. Observed scales at supercritical shocks /19/.

length $L_{CIIL,1} = V_{xL}/\Omega_{ciL} \simeq 560$km. The modeling of BG illustrated in Figure 24 has compressed the shock transition (with all of these components in it) into the ramp scale! This is a 40:1 compression of scales in the BG model versus reality! In addition, the modeling of BG used the $B_y(x')$ profile to make the overshoot of |B| (cf. Fig. 24), disregarding the published and well-known correlation of the overshoot in |B| with B_z and V_{yi} of the gyrating ions behind the shock. Since from equation (3) the NI electric field goes like $d/dx(B^2/8\pi)$, the ad hoc placement and size of $B_y(x')$ affects the NI electric field, placing this coherent pulse in the ramp making the Hugoniot transitions, exacerbates the gradient of E. Manipulating the B profile with a B_y signature that is comparable to B_z is also unwarranted and not seen in the data. Figure 25 from reference /44/, shows the out-of-plane component locations and the overall intensity of B, and it is relatively small. While the observed B_y signatures are in the ramp, they do not compete with the amplification of B_z to make |B| increase either in subcritical or supercritical shocks or to form the overshoots.

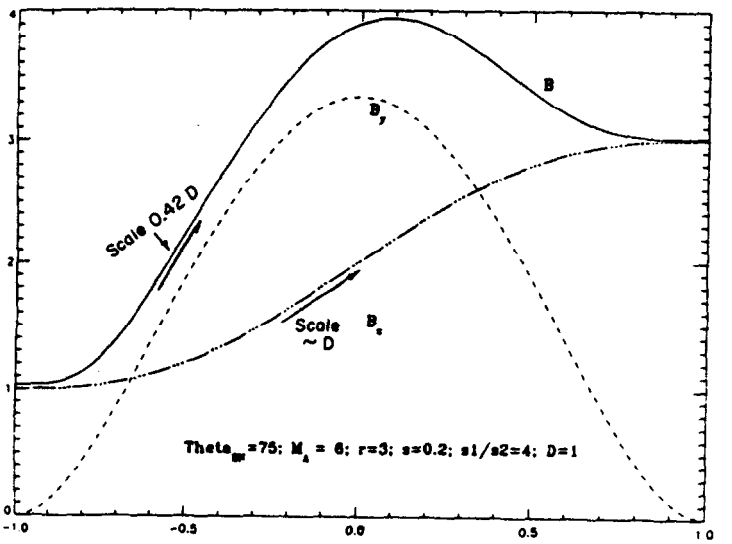

Fig. 24. Ad hoc model of oblique supercritical transition /34/. Horizontal axis is spatial axis between $-1 \leq x/\mathrm{D} \leq 1$.

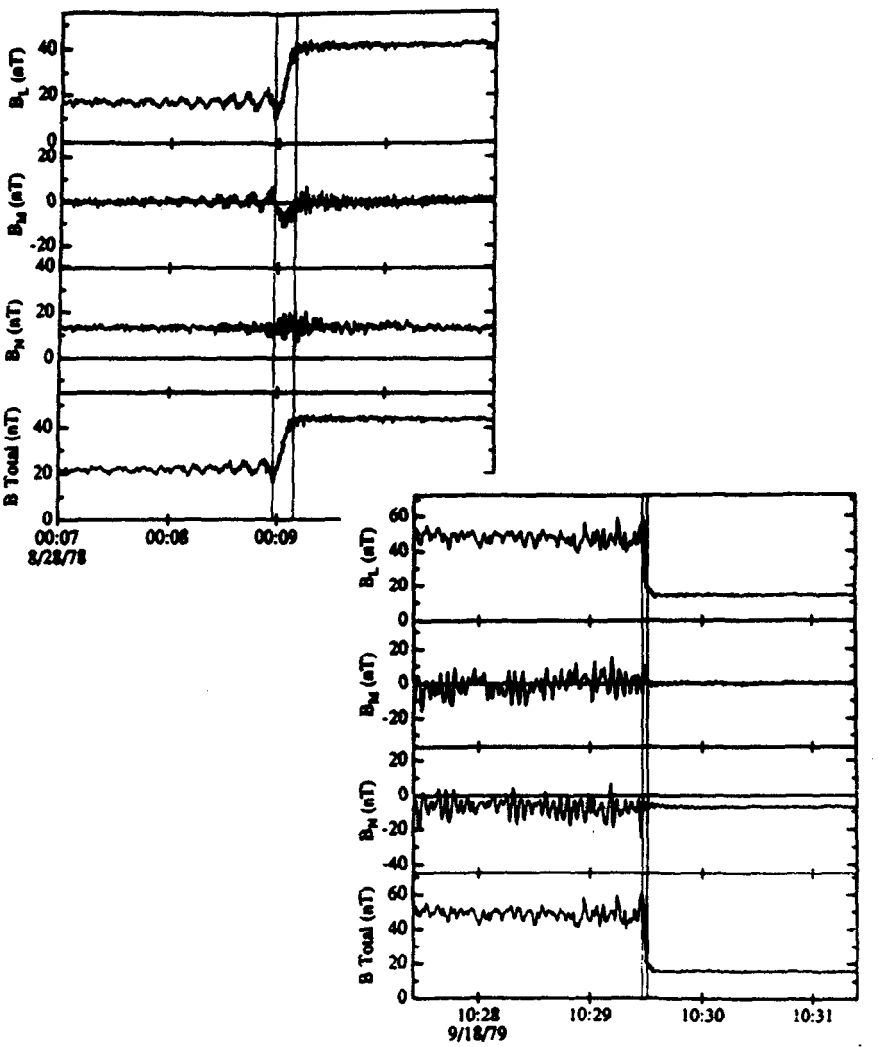

Fig. 25. Size of B_y, B_m features in observed resistive and supercritical shocks /44/.

SUMMARY

In the post-ISEE era, the coherent forces within the shock layer are seen to be the most efficient and in some cases the only viable approach for implementing the shock layer transitions in ions *and* electrons on the now documented spatial scales. Microinstabilities take too long to develop to be the primary vehicle for momentum transfer from normal to transverse directions. Long before they can amplify sufficiently to heat the ions of the plasma, the ions have hurdled over the layers where the free energy is imagined to be present. The observed currents are too weak to play a role in microsinstability "heating" of the electrons. The electron dispersion (moment temperature) is principally determined by the guiding center ordered inflation in phase space of the solar wind distribution as it is accelerated through the HT potential drop and as the particles move into the differing downstream magnetic intensity. This is a DC effect and explains why the electron parallel and perpendicular pressures respond so "promptly" and nearly equally in strong shocks to the change of state signaled by the field profile and the HT potential jump. By contrast, the coherent DC electric and magnetic forces within the layers are now viewed as the first-order mediators that convert directed momentum or Poynting flux into nondirected plasma energy, loosely called downstream pressure.

Realizing what these zero-frequency forces can do to a supersonic ion and subsonic electron distribution is the principal new insight into the shock layer physics made possible by the recent data from the ISEE and AMPTE missions. Some of these generic effects have been studied theoretically to see what kinds of coherent energy rearrangements are possible with these forces. On rather general grounds, for example, it has been shown /36/ (i) that accelerating potentials can increase the temperature of the accelerated species if it is initially subsonic as are the electrons, and (ii) that deceleration of a supersonic species will also increase its temperature in the direction along the deceleration. In the process of writing this review, the preferential perpendicular inflation of $f(\mathbf{v})$ for electrons at weak shocks was also explained as a natural outcome of the coherent guiding center ordered DC forces in the shock layer. The same coherent physics provides a nearly isotropic "inflation" of $f_e(v)$ at stronger shocks as a different extreme of a continuum of DC effects more nearly relevant for strong shocks such as the planetary bow shocks. Nonguiding center ordered descriptions at shocks remains an unsubstantiated hypothesis. Wave particle effects appear to round the corners on the distribution functions or fill voids, but the primary repartition of directed to nondirected energy seems to be controlled by these zero-frequency forces.

While hybrid simulations with particle ions and fluid electrons have played an important role in the understanding of the nonguiding center gyro-mechanics of the ions near the collisionless shocks of space (cf. reviews /22,63/), the understanding of electron physics has evolved, until very recently, from observational surveys and the guiding center ordered analytical work that is possible when the electrons of the upstream plasma can be idealized as magnetized throughout the shock layer. Only the most recent simulations of Savoini and Lembege /45/ have finally recovered the electron flat-top morphology while self-consistently determining the shock profile. Only this simulation has finally been able to confirm the painstaking experimental work summarized above. With their diagnostics, Savoini and Lembege have reaffirmed the reviewed experimental arguments of the overwhelming importance for electrons of the DC fields in the inflation of $f_e(\mathbf{v})$ and the physics of their "heating" at collisionless shocks.

REFERENCES

1. C. C. Goodrich and J. D. Scudder, The adiabatic energy change of plasma electrons and the frame dependence of the cross shock potential at collisionless magnetosonic shock waves, *J. Geophys. Res.*, 89, 6654 (1984).

2. F. deHoffmann and E. Teller, Magnetohydrodynamic shocks, *Phys. Rev.*, 80, 692 (1950).

3. M. D. Montgomery, J. R. Asbridge and S. J. Bame, Vela 4 plasma observations near the Earth's bow shock, *J. Geophys. Res.*, 75, 1217 (1970).

4. J. D. Scudder, D. Lind and K. W. Ogilvie, Electron observations in the solar wind and the magnetosheath, *J. Geophys. Res.*, 78, 6535 (1973).

5. A. A. Galeev, Collisionless shocks, in: *Physics of Solar Planetary Environments*, ed. D. Williams, AGU, Washington DC, 1976, p. 464.

6. R. Z. Sagdeev, Cooperative phenomena and shock waves in collisionless plasmas, in: *Reviews of Plasma Physics*, ed. M. A. Leontovitch, Consultants Bureau, New York, 1966, p. 23.

7. M. H. Acuña, L. F. Burlaga, R. P. Lepping and N. F. Ness, Initial results from Voyager 1,2 magnetic field experiments, Proc. *4th Solar Wind Conference*, ed. H. Rosenbauer, MPAE-W-100-81-31, 1981, p. 143.

8. J. D. Scudder, L. F. Burlaga and E. W. Greenstadt, Scale lengths in quasi-parallel shocks, *J. Geophys. Res.*, 89, 7545 (1984).

9. W. C. Feldman, Electron heating at interplanetary shocks, in: *Solar Wind 5*, ed. M. Neugebauer, NASA CP2280, 1983.

10. M. F. Thomsen, M. M. Mellott, J. A. Stansberry, S. J. Bame, J. T. Gosling and C. T. Russell, Strong electron heating at the Earth's bow shock, *J. Geophys. Res.*, 92, 10,119 (1987).

11. S. J. Schwartz, M. F. Thomsen, W. C. Feldman and F. T. Douglas, Electron dynamics and potential jump across slow mode shocks, *J. Geophys. Res.*, 92, 3165 (1987).

12. C. T. Russell, M. M. Hoppe, W. A. Livesey, J. T. Gosling and S. J. Bame, ISEE 1-2 observations of Laminar bow shocks: Velocity and thickness, *Geophys. Res. Lett.*, 9, 1171 (1982).

13. W. C. Feldman, S. J. Bame, S. P. Gary, J. T. Gosling, D. J. McComas, M. F. Thomsen, G. Paschmann, N. Sckopke, M. M. Hoppe and C. T. Russell, Electron heating by field aligned free energy within the Earth's bowshock, *Phys. Rev. Lett.*, 49, 199 (1982).

14. W. C. Feldman, R. C. Anderson, S. J. Bame, S. P. Gary, J. T. Gosling, D. J. McComas, M. F. Thomsen, G. Paschmann and M. M. Hoppe, Electron velocity distributions near the Earth's bow shock, *J. Geophys. Res.*, 88, 96 (1983).

15. M. Leroy and A. Mangeney, A theory of energization of solar wind electrons by the Earth's bow shock, *Ann. Geophys.*, 2 (4), 449 (1984); also C. S. Wu, A fast Fermi process: Energetic electrons accelerated by a nearly perpendicular bow shock, *J. Geophys. Res.*, 89, 8857 (1984).

16. R. J. Fitzenreiter, A. J. Klimas and J. D. Scudder, Detection of bump on tail reduced distribution functions at the electron foreshock boundary, *Geophys. Res. Lett.*, 11, 496 (1984).

17. R. J. Fitzenreiter, J. D. Scudder and A. J. Klimas, Three dimensional analytical model for the spatial variations of the foreshock electron distribution function: Systematics and comparisons with ISEE observations, *J. Geophys. Res.*, 95, 4155 (1990).

18. R. J. Fitzenreiter, The Earth's foreshock, 1994 COSPAR review, this issue.

19. J. D. Scudder, A. Mangeney, C. Lacombe, C. C. Harvey, T. L. Aggson, R. R. Anderson, J. T. Gosling, G. Paschmann and C. T. Russell, The resolved layer of a collisionless, high β, supercritical, quasi-perpendicular shock wave: 1. Rankine-Hugoniot geometry, currents and stationarity, *J. Geophys. Res.*, 91, 11,019-11,052 (1986).

20. M. F. Thomsen, H. C. Barr, S. P. Gary, W. C. Feldman and T. E. Cole, Stability of electron distributions within the Earth's bow shock, *J. Geophys. Res.*, 88, 3035 (1983).

21. M. M. Leroy, C. C. Goodrich, D. Winske, C. S. Wu and K. Papadopoulos, Simulations of a perpendicular bow shock, *Geophys. Res. Lett.*, 8, 1269, (1981); M. M. Leroy, D. Winske, C. C. Goodrich, C. S. Wu and K. Papdopoulos, The structure of perpendicular bow shocks, *J. Geophys. Res.*, 87, 5081 (1982).

22. C. C. Goodrich, Numerical simulations of quasi-perpendicular collisionless shocks, in: *Collisionless Shocks in the Heliosphere: Reviews of Current Research*, eds. B. T. Tsuritani and R. G. Stone, AGU, Washington DC, 1985.

23. J. D. Scudder, A. Mangeney, C. Lacombe, C. C. Harvey and T. L. Aggson, The resolved layer of a collisionless, high β, supercritical, quasi-perpendicular shock wave: 2. Dissipative electrodynamics. *J. Geophys. Res.*, 91, 11,053-11,073 (1986).

24. J. D. Scudder, A. Mangeney, C. Lacombe, C. C. Harvey, C. S. Wu and R. R. Anderson, The resolved layer of a collisionless, high β, supercritical, quasi-perpendicular shock wave: 3. Vlasov electrodynamics, *J. Geophys. Res.*, 91, 11,074-11,097 (1986); cf. also S. J. Schwarz, Comment on "The resolved layer of a collisionless, high β, supercritical, quasi-perpendicular shock wave: 3. Vlasov electrodynamics, by J. D. Scudder, A. Mangeney, C. Lacombe, C. C. Harvey, C. S. Wu and R. R. Anderson," *J. Geophys. Res.*, 92, 6171 (1987); and J. D. Scudder, Reply to Schwarz, *J. Geophys. Res.*, 92, 6169 (1987).

25. C. C. Goodrich and J. D. Scudder, Reply (to reference /26/), *J. Geophys. Res.*, 91, 7135 (1986).

26. R. A. Cairns, Comment on "The adiabatic energy change of plasma electrons and the frame dependence of the cross shock potential at collisionless magnetosonic shock waves," by C. C. Goodrich and J. D. Scudder, *J. Geophys. Res.*, 91, 7134 (1986).

27. D. A. Tidman and N. A. Krall, *Shock Waves in Collisionless Plasmas*, J. Wiley Interscience, New York, 1971, p. 59ff, also Chapter 5.

28. J. R. Wygant, M. Bensadoun and F. S. Mozer, Electric field measurements at subcritical oblique bow shock crossings, *J. Geophys. Res.*, 92, 11,109 (1987).

30. H. Alfvén, and C. G. Fälthammer, *Cosmical Electrodynamics*, 2d ed., Clarendon Press, Oxford, 1963.

31. E. C. Whipple, The signature of parallel electric fields, *J. Geophys. Res.*, 82, 1525 (1978).

32. W. C. Feldman, Electron velocity distributions near collisionless shocks, in: *Collisionless Shocks in the Heliosphere: Reviews of Current Research*, eds. B. T. Tsuritani and R. G. Stone, AGU, Washington DC, 1985.

33. J. D. Scudder, The field aligned flow approximation for electrons within layers possessing a normal mass flux: A corollary to the deHoffmann Teller theorem, *J. Geophys. Res.*, 92, 13,447, (1987).

34. M. Balikhin and M. Gedalin, Kinematic mechanism of electron heating in shocks: Theory vs observations, *Geophys. Res. Lett.*, 21, 841 (1994).

35. J. D. Scudder, Balatonfured meeting on Collisionless Shocks, *EOS* (1987).

36. J. D. Scudder, On the causes of temperature change in inhomogeneous low density astrophysical plasmas, *Astrophys. J.*, 398, 299-318 (1992).

37. P. Veltri, A. Mangeney and J. D. Scudder, Electron heating in quasi-perpendicular shocks: A Monte Carlo simulation, *J. Geophys. Res.*, 95, 14,939 (1990).

38. R. L. Morse, Adiabatic time development of plasma sheaths, *Phys. Fluids*, 8, 308 (1965).

39. M. F. Thomsen, J. T. Gosling, S. J. Bame, K. B. Quest, D. Winske, W. A. Livesey and C. T. Russell, On the noncoplanarity of the magnetic field within fast collisionless shocks, *J. Geophys. Res.*, 92, 2305 (1987).

40. F. Jones and D. Ellison, Noncoplanar magnetic fields, shock potentials and ion deflection, *J. Geophys. Res.*, 92, 11,205 (1987).

41. J. T. Gosling, D. Winske and M. Thomsen, Noncoplanar magnetic fields at collisionless shocks: Test of a new approach, *J. Geophys. Res.*, 93, 2735 (1988).

42. M. A. Freidman, C. T. Russell, J. T. Gosling and M. F. Thomsen, Noncoplanar component of the magnetic field at low Mach number shocks, *J. Geophys. Res.*, 95, 2441 (1990).

43. F. Jones and D. Ellison, The plasma physics of shock acceleration, *Space Sci. Rev.*, 58, 259 (1991).

44. M. H. Farris, C. T. Russell and M. F. Thomsen, Magnetic structure of the low beta quasi-perpendicular shock, *J. Geophys. Res.*, 98, 15,285 (1993).

45. P. Savoini and B. Lembege, Electron dynamics in two and one dimensional oblique supercritical collisionless magnetosonic shocks, *J. Geophys. Res.*, 99, 6609-6635 (1994).

46. A. Jeffrey and T. Taniuti, *Non-Linear Wave Propagation with Applications to Physics and Magnetohydrodynamics*, Academic Press, New York, 1964.

47. B. Rossi and S. Olbert, *Introduction to the Physics of Space*, McGraw Hill Book Co., New York, 1970.

48. W. C. Feldman, S. J. Schwarz, S. J. Bame, D. N. Baker, J. Birn, J. T. Gosling, E. W. Hones, Jr., D. J. McComas, J. A. Slavin, E. J. Smith and R. D. Zwickl, Evidence for slow mode shocks in the distant geomagnetic tail, *Geophys. Res. Lett.*, 11, 599 (1984).

49. W. C. Feldman, D. N. Baker, S. J. Bame, J. Birn, J. T. Gosling, E. W. Hones, Jr., S. J. Schwarz and R. D. Zwickl, Slow mode shocks: Semipermanent feature of the distant geomagnetic tail, *J. Geophys. Res.*, 90, 233 (1985).

50. W. C. Feldman, R. L. Tokar, J. Birn, E. W. Hones, Jr., S. J. Bame and C. T. Russell, Structure of a slow mode shock observed in the plasma sheet boundary layer, *J. Geophys. Res.*, 92, 83 (1987).

51. D. W. Walthour, J. T. Gosling, B.U.Ö. Sonnerup and C. T. Russell, Observations of anomalous slow-mode shock and reconnection layer in the dayside magnetopause, *J. Geophys. Res.*, submitted 1994.

52. J. K. Chao and S. Olbert, Observations of slow shocks in the interplanetary medium, *J. Geophys. Res.*, 75, 6394 (1970).

53. W. P. Wilkinson, Ion kinetic processes and thermalization at quasi-perpendicular low Mach number shocks, *J. Geophys. Res.*, 96, 17,675 (1991).

54. M. F. Thomsen, J. T. Gosling, S. J. Bame, M. M. Mellott, Ion and electron heating at collisionless shocks near the critical Mach number, *J. Geophys. Res.*, 90, 137 (1985).

55. D. W. Forslund and C. R. Shonk, Formation and structure of electrostatic collisionless shocks, *Geophys. Res. Lett.*, 25, 1699 (1970).

56. C. T. Dum, R. Chodura and D. Biskamp, Turbulent heating and quenching of the ion sound instability, *Phys. Rev. Lett.*, 32, 1231 (1974).

57. D. W. Forslund, K. B. Quest, J. U. Brackbill and K. Lee, Collisionless dissipation in quasi-perpendicular shocks, *J. Geophys. Res.*, 89, 2142 (1984.)

58. D. M. Winske, Y. Tanaka, C. S. Wu and K. B. Quest, Plasma heating at collisionless shocks due to the kinetic cross field streaming instability, *J. Geophys. Res.*, 90, 123 (1985).

59. S. J. Schwartz, M. F. Thomsen, S. J. Bame, J. T. Stansberry, Electron heating and the potential jump across fast mode shocks, *J. Geophys. Res.*, 93, 12,923 (1988).

60. R. L. Tokar, C. H. Aldrich, D. W. Forslund and K. B. Quest, Non-adiabatic electron heating at high Mach number perpendicular shocks, *Phys. Rev.*, 56, 1059 (1986).

61. M. Balikhin, M. Gedalin and A. Petrukovich, New mechanism for electron heating in shocks, *Phys. Rev. Lett.*, 70, 1259-1262 (1993).

63. K. Cole, Effects of cross magnetic and (spatially dependent) electric fields on charged particle motions, *Planet. Space Sci.*, 24, 515 (1976).

64. J. T. Gosling and A. E. Robson, Ion reflection, gyration, and dissipation at supercritical shocks, in: *Collisionless Shocks in the Heliosphere: Reviews of Current Research*, eds. B. T. Tsuritani and R. G. Stone, AGU, Washington DC, 1985.